

1 **Research article**2 **Cross-scale environmental impacts across persistent and**
3 **dynamic aggregations within a complex population:**
4 **implications for fisheries management**5 Georgios Kerametsidis^{1,2,*}, James Thorson³, Vincent Rossi⁴, Diego Álvarez-
6 Berastegui¹, Cheryl Barnes⁵, Gregoire Certain⁶, Antonio Esteban⁷, Encarnación
7 García⁷, Angélique Jadaud⁶, Safo Piñeiro¹, Miguel Vivas⁷, Manuel Hidalgo¹8 ¹*Centro Oceanográfico de Baleares (IEO, CSIC), Moll de Ponent s/n, 07015, Palma, Balearic Islands,*
9 *Spain,* ²*University of the Balearic Islands, Carretera de Valldemossa, km 7.5, 07122, Palma, Balearic*
10 *Islands, Spain,* ³*Habitat and Ecological Processes Research Program, Alaska Fisheries Science Center,*
11 *NOAA, Seattle, WA, USA,* ⁴*Mediterranean Institute of Oceanography (UM110, UMR 7294), CNRS, Aix*
12 *Marseille Univ., Univ. Toulon, IRD, Marseille, France,* ⁵*Department of Fisheries, Wildlife, and*
13 *Conservation Sciences, Oregon State University, Newport, OR, USA.* ⁶*MARBEC, Univ. Montpellier,*
14 *CNRS, Ifremer, IRD, Sète, France,* ⁷*Centro Oceanográfico de Murcia (IEO-CSIC), C/ Varadero, 1,*
15 *30740 Lo Pagan, Murcia, Spain*16 *Corresponding author: tel: +34 971 133 720; e-mail: georgios.kerametsidis@ieo.csic.es /
17 georgios.kerametsidis@uib.eu18 **ABSTRACT**19 Accounting for marine stocks spatiotemporal complexity has become one of the most pressing
20 improvements that should be added to the new generation of stock assessment. Disentangling
21 persistent and dynamic population subcomponents and understanding their main drivers of
22 variation are still stock-specific challenges. Here, we hypothesized that the spatiotemporal
23 variability of two adjacent fish stocks density is associated with spatially structured
24 environmental processes across multiple spatiotemporal scales. To test this, we applied a
25 generalized Empirical Orthogonal Function and Dynamic Factor Analysis to fishery-

26 independent and -dependent data of red mullet, a highly commercial species, in the Western
27 Mediterranean Sea. Areas with persistent and dynamic high aggregations were detected for both
28 stock units. A large-scale climatic index and local open-ocean convection were associated with
29 both stocks while other variables exhibited stock-specific effects. We also revealed spatially
30 structured density dynamics within the examined management units. This suggests a
31 metapopulation structure and supports the future implementation of a spatial stock assessment.
32 Considering the common assumptions of panmictic structure and absence of connectivity with
33 neighbouring stock units, our methodology can be applied to other species and systems with
34 putative spatial complexity to inform a more accurate structure of biological populations.

35 **Keywords:** *Mullus barbatus*, empirical orthogonal function, dynamic factor analysis,
36 Mediterranean Sea, open-ocean convection, stock identification

37 1. Introduction

38 Understanding species spatiotemporal distributions and densities is critical to linking ecological
39 mechanisms and conservation measures. For commercially exploited species, obtaining
40 information about the spatiotemporal dynamics of their distribution and density is a prerequisite
41 to providing robust management advice (Rufener et al. 2021) while it is also central to the
42 Ecosystem-Based Fisheries Management (EBFM). EBFM is widely viewed as a set of tools for
43 successful management in different contexts (Trochta et al. 2018) and constitutes a fundamental
44 component of sustainability and balance between environmental, social and economic
45 objectives (Marshall et al. 2018). Current stock assessment frameworks often do not include
46 key features such as ecosystem components and ecological complexity of populations although
47 it has already been shown that environmental and climatic variation are closely associated with
48 the abundance variation of commercially important species (e.g. Schlenker et al. 2023).
49 However, the ongoing development of next-generation stock assessments highly prioritizes the
50 incorporation of missing critical information (Punt et al. 2020). This inherently requires the
51 identification of spatial structure to model more realistic population dynamics and develop

52 reliable assessment and management frameworks (Punt 2019; Punt et al. 2020). Despite the
53 recognition of complex spatial structures in many stocks (Reiss et al. 2009; Matic-Skoko et al.
54 2018; Hidalgo et al. 2019a), management unit boundaries are not yet generally reconciled, and
55 stock assessments rely on the assumption of single panmictic stocks for the majority of
56 resources. A plethora of studies have shown that not accounting for spatial complexity can
57 unintentionally lead to overfishing with often devastating consequences for the stocks (Goethel
58 and Berger 2016; Kerr et al. 2017; Cadrin 2020; Punt 2023). Conversely, modeling studies
59 suggest that incorporating spatial complexity improves the performance of population models
60 used in stock assessment (Goethel et al. 2011, 2021; Punt 2019).

61 A stock unit is generally defined as a subset of the whole population of a species that shares the
62 same growth, recruitment, spawning and mortality characteristics and inhabits the same
63 geographic area (Sparre and Venema 1998). However, all these biological parameters and
64 processes can exhibit non-stationary relationships with environmental variables. Not
65 accounting for the latter may result in unrealistic outputs of the fisheries assessment models,
66 which can hamper efficient fisheries management. This risk is even more pronounced in stocks
67 with complex spatial structures where local environmental drivers may differ across different
68 stock subunits. As an essential component of local habitats, dynamic environmental conditions
69 can result in spatial restructuring of the stocks with further demographic implications
70 (Szuwalski and Hollowed 2016; Kerr et al. 2017). The environment influences critical
71 ecological processes such as recruitment (Houde 2016), spawning (Di Stefano et al. 2023) or
72 mortality (Kerametsidis et al. 2023), as well as several life history parameters of fish, such as
73 growth or reproductive scheduling (Perry et al. 2005.; Clark et al. 2020). In fact, in some cases,
74 no clear stock-recruitment patterns can be evidenced, which leaves the environment as the main
75 driver of recruitment with minimal influence of the spawning stock (Szuwalski et al. 2015;
76 Hidalgo et al. 2019b). Therefore, considering the spatial heterogeneity that exploited stocks are
77 subject to, the hypothesis that spatially structured environmental processes (i.e. environmental

78 processes varying across multiple spatial scales) explain critical ecological and demographic
79 processes seems plausible and needs to be explored.

80 Various life stages and traits are linked to cross-scale environmental processes (Twinaime et al.
81 2020), and thus both fine- and broad-scale environmental processes must be considered to
82 properly comprehend the full life cycle of fish. Complex spatiotemporal variation among local
83 habitats is often aggregated into broader-scale measurements such as climate indices (Stenseth
84 and Myrseterud 2005; Thorson et al. 2020a). Besides this cross-scale nature of environmentally
85 driven processes, there are other important factors to consider when investigating the dynamics
86 of animal populations. These include movements towards favourable habitats and persistent
87 climatically and environmentally driven population hotspots. Hence, providing a mechanistic
88 understanding of the links between environmental and density variability in space and time is
89 essential, particularly for commercial stocks. This is especially critical considering the current
90 climate change scenarios (e.g. Lotze et al. 2019) and environment-driven shifts in density and
91 distribution that have been noted for a variety of organisms within the marine realm (Bowler et
92 al. 2017; Champion et al. 2021; Thorson et al. 2021).

93 More than 30% of fish stocks are exploited beyond biologically sustainable limits globally
94 (FAO 2022a). In certain basins, this percentage might be considerably higher. For instance,
95 73% of all fish stocks are overexploited in the Mediterranean Sea (FAO 2022b). Despite the
96 recent implementation of highly promising management plans, such as the Multiannual Plan
97 for Demersal fish stocks in the western Mediterranean Sea (Sánchez Lizaso et al. 2000), there
98 are still issues inhibiting the proper management of commercial stocks (Cardinale et al. 2021).

99 While recent studies have recommended larger species-specific units for the better assessment
100 of some Mediterranean stocks (e.g. Fiorentino et al. 2015; Spedicato et al. 2021; STECF 2021),
101 there is also cumulative evidence of the importance of local and regional dynamics (Hidalgo et
102 al. 2019b; Paradinas et al. 2022) challenging these recommendations and encouraging the
103 implementation of spatially structured stock assessment frameworks (Cadrin 2020; Punt 2023).

104 Obtaining high-resolution information on population spatial structure and connectivity is a

105 prerequisite for spatial stock assessments (Goethel et al. 2023) and is logistically feasible for
106 data-rich species and systems.

107 For stocks with long, adequate and spatially resolved time series of fishery-dependent and -
108 independent data, scientists and stakeholders might be benefited from analyzing spatiotemporal
109 patterns and/or connectivity between different stock units. In this study, we used red mullet
110 (*Mullus barbatus*, Linnaeus, 1758) in the north-western (NW) Mediterranean Sea as a case
111 study, where its populations have been historically managed in two separate units, the Northern
112 Spanish Coast and the Gulf of Lions. We hypothesized that the spatiotemporal variability
113 among and within the two management units would be associated with specific spatially
114 structured environmental processes across multiple scales. To test this hypothesis, we first
115 described persistent and dynamic density hotspots and then we identified the environmental
116 variables that drive the spatiotemporal variability of red mullet density across different areas.
117 We employed a two-fold spatiotemporal approach: *i*) we used abundance-sampling data from
118 scientific trawling to explore the principal modes of density variability, the persistent density
119 hotspots as well as putative environmental drivers of the spatiotemporal variability in the two
120 management units, and *ii*) we analyzed monthly landings per unit effort (LPUE) data from
121 commercial fishing operations to explore whether the seasonal and long-term trends are
122 spatially structured.

123 **2. Materials and methods**

124 *2.1. Target area & species*

125 Our study area encompasses two management units that are used by the General Fisheries
126 Commission for the Mediterranean: the Northern Spanish Coast (Geographic Sub-Area (GSA)
127 06) and the Gulf of Lions (Geographic Sub-Area (GSA) 07) in the NW Mediterranean and
128 covers the trawlable waters of these areas (Fig. 1).

129 *Mullus barbatus* (hereafter referred to as red mullet) is a demersal fish distributed in the eastern
130 Atlantic Ocean, from the North Sea to Senegal, and throughout the Mediterranean and Black

131 Seas (Fischer et al. 1987). Red mullet commonly resides over soft sandy and muddy substrates
132 and is mainly distributed along the continental shelf in depths of up to 300 to 400 m, with
133 significant declining trends in waters deeper than 200 m (Tserpes et al. 2019). It is a high-value
134 commercial species and one of the most important and overexploited resources in
135 Mediterranean demersal fisheries, predominantly targeted by bottom-trawl fisheries. It is one
136 of the two demersal fish species that have long been assessed separately on an annual basis in
137 the GSA06 and GSA07 while a complex demographic structure partially shaped by the elevated
138 dispersal abilities in early life stages has been evidenced in other regions (Gargano et al. 2017).
139 In the Western Mediterranean Sea, three spatially segregated and persistent density hotspots
140 have been detected along the Northern Spanish Coast in the Mediterranean Sea (i.e. within the
141 management unit GSA06) (Paradinas et al. 2020). This might indicate a more complex
142 population structure resembling that of a metapopulation system, as suggested for other
143 harvested species in the Mediterranean Sea (Hidalgo et al. 2019a; Gargano et al. 2022).

144 2.2. Data sources

145 2.2.1. Biological data

146 Data on red mullet were obtained from two different sources to apply two complementary
147 modelling approaches: (1) standardised density data from scientific trawling and (2) landings
148 per unit effort (LPUE) from commercial fisheries. Annual standardised abundance data for
149 GSA06 & GSA07 were collected during the EU-funded International Mediterranean Bottom
150 Trawl Survey (MEDITS) that was carried out between spring and early summer (April to June)
151 between 1994 and 2019 (Anonymous 2017; Spedicato et al. 2019). The MEDITS project
152 follows a stratified sampling design based on the coverage of five bathymetric strata (10–50,
153 51–100, 101–200, 201–500 and 501–800 m) in each Mediterranean GSA and uses a GOC-73
154 net with a 20 mm mesh size. Sampling stations were randomly placed within each stratum at
155 the beginning of the project and in all subsequent years, sampling was carried out in similar
156 randomized locations. The duration of the hauls has been specified to 30 min in depths of <200
157 m and to 60 min in >200m waters. Since the abundance of red mullet declines significantly

158 over 200 m (Tserpes et al. 2019), data from hauls deeper than 200 m were excluded from this
159 study. Preliminary analysis confirmed this declining trend in our dataset. A total of 1499 and
160 1419 trawl operations were observed over a period of 26 years, averaging 58 and 55 fishing
161 hauls per year for the GSA06 and the GSA07, respectively. Mean densities were approximately
162 651 and 494 ind. km⁻² haul⁻¹ in the GSA06 and GSA07, respectively, and red mullet was
163 encountered in 47% to 93% of hauls in each year in both areas.

164 Since MEDITS only takes place during a short prespecified period in late spring/early summer,
165 monthly LPUE (during 2004-2019) from commercial fishing operations were used as a
166 complementary data source to capture the intra- and inter-annual density variability. Monthly
167 LPUE were standardized considering the number of vessels and the number of fishing days per
168 month to make data from different ports comparable as landings in kg per fishing trip (Puerta
169 et al. 2016). Fishing operations in the area are always developed on a daily basis within short
170 distances from the port. LPUE data were used to explore the dynamics across the GSA06 as
171 previous studies have already proposed three persistent hotspots for the species in GSA06
172 (Paradinas et al. 2020). LPUE data for the GSA07 were not available. There are 52 ports with
173 commercial fisheries operations in the GSA06, however, only those ports for which landing
174 data were available for at least 10 months, of which 6 consecutive, every year during 2004-
175 2019 were selected to be included in our analyses. The selected ports were grouped based on
176 the three known aggregations: the area south of Valencia Channel, the area north of Valencia
177 Channel and the Catalan Coast (Fig. 1). In addition, to closely capture the dynamics in the
178 persistent and dynamic density hotspots of the species (see section 2.3.1), only ports near the
179 Ebro Delta area (north of Valencia Channel) and in the very south of the area south of Valencia
180 Channel were retained. After applying the above criteria, a total of 20 ports were included in
181 the LPUE analyses (Fig. 1).

182 2.2.2. Environmental data

183 Eight environmental indices with known influence in the same region and other species were
184 utilized in the present study (Table 1, Supplementary materials S1). To capture the effects of

185 broad-scale coupled atmosphere-ocean climatic processes, three indices were used. Data on the
186 Atlantic Multidecadal Oscillation (AMO) and the North Atlantic Oscillation (NAO) were
187 downloaded from the National Oceanic and Atmospheric Administration (NOAA, Physical
188 Sciences Laboratory: <https://www.psl.noaa.gov/data/correlation/amon.us.long.data> &
189 [https://www.cpc.ncep.noaa.gov/products/precip/CWlink/pna/norm.nao.monthly.b5001.curren
190 t.ascii.table](https://www.cpc.ncep.noaa.gov/products/precip/CWlink/pna/norm.nao.monthly.b5001.current.ascii.table), accessed on February 2022). AMO represents changes in the sea surface
191 temperature (SST) in the North Atlantic Ocean from 0° to 70° N that are characterized by
192 multidecadal variability (Dijkstra et al. 2006; Knight et al. 2006). A negative AMO phase is
193 associated with an anomalously low North Atlantic SST. Several impacts of AMO on climate
194 (Knight et al. 2006) and the fish communities of the NE Atlantic (Zimmermann et al. 2019)
195 and the Mediterranean Sea (Tsikliras et al. 2019) have been documented, including influence
196 on recruitment success and community ratios. Second, the North Atlantic Oscillation (NAO)
197 was employed. NAO represents an alternation in pressure between the subtropic atmospheric
198 high-pressure zone centered over the Azores and the atmospheric low-pressure zone over
199 Iceland. A positive phase of NAO results in a higher frequency and stronger winter storms
200 crossing the Atlantic Ocean in a more northerly track. Inversely, a negative phase of NAO is
201 associated with fewer and weaker winter storms crossing on a more west-east pathway
202 (Ottersen et al. 2001). Finally, we used the Western Mediterranean Oscillation index (WeMOi),
203 which is defined as the difference in the standardized values in sea level pressures between
204 Cádiz-San Fernando (Spain) and Padua (Italy) (Martin-Vide and Lopez-Bustins 2006), has been
205 shown to influence fish species in the Western Mediterranean (Martín et al. 2012). Data on
206 WeMOi were obtained from the Climatology Group of the University of Barcelona
207 (http://www.ub.edu/gc/documents/Web_WeMOi-2019.txt, accessed in February 2022).

208 Surface chlorophyll-a (chl-a) concentration was used as a proxy of primary productivity and
209 sea surface temperature (SST) was used to inform the regional thermal conditions in each
210 management unit over two contrasting seasons. For both variables, seasonal spatial averages
211 corresponding to winter (December-February) and late spring/summer (May-July) were

212 computed. In order to assess the influence of these two variables on a local scale and specifically
213 on the aggregations in GSA06, besides an average for the whole GSA06, seasonal spatial
214 averages were also calculated for the subareas of Catalan Coast, the Ebro Delta and the Valencia
215 Channel (Fig. 1). For the GSA07, only the unique spatial average for the whole region was
216 calculated and used. Data on chl-a and SST were downloaded from the E.U. Copernicus Marine
217 Service (chl-a: <https://doi.org/10.48670/moi-00300>, SST: [https://doi.org/10.25423/CMCC/
218 MEDSEA_MULTIYEAR_PHY_006_004_E3R1](https://doi.org/10.25423/CMCC/MEDSEA_MULTIYEAR_PHY_006_004_E3R1)). Further, a Local Climatic Index (LCI) was
219 also included. LCI quantifies an integrated hydroclimatic variability at the regional scale,
220 synthesizing the air temperature, sea surface temperature, atmospheric sea level pressure, 500
221 hPa geopotential height, and precipitation rates at a monthly scale by means of the first axis of
222 a Principal Component Analysis (Molinero et al. 2005). Positive LCI values are associated with
223 higher regional atmospheric sea level pressure and 500 hPa geopotential height, whereas
224 negative values are associated with high precipitation rate. The Ebro River runoff (m^3s^{-1}),
225 calculated at its mouth, was also included in the study as a proxy of the nutrient discharge from
226 the river into the sea (Ebro Hydrographic Confederation, <https://www.chebro.es/>). Sea Bottom
227 Temperature (SBT) was not included in this study as it is generally more conservative than
228 temperatures in the rest of the water column (Hiddink and ter Hofstede 2008). Specifically, for
229 GSA06 and GSA07 combined, we examined the monthly average SBT from 1992 to 2019 and
230 we found very little monthly variation (i.e. mean SBT ranging from 12.8 to 13.5 °C) and we
231 therefore decided to exclude it from the rest of the analyses.

232 Finally, we also assessed the potential influence of open-ocean convection in the NW
233 Mediterranean, as observed in other species (Martin et al. 2016; Hidalgo et al. 2019a). This
234 phenomenon, whose magnitudes and extents vary over time (Houpert et al. 2016), occurs during
235 winter, typically between December and March, mainly in the Gulf of Lions and off the
236 northern Catalan coast (Fig. 1). It is associated with the regional incidence of northerly cold
237 and dry winds, and local oceanographic features, which favours winter vertical mixing and
238 deepening of the mixed layer. During some years, atmospheric forcing can be particularly

239 strong, and stratification erosion can reach great depths or even the seafloor (Mertens and Schott
240 1998). Open-ocean deep convection is a major regional oceanographic process, which greatly
241 contributes to the primary productivity and nutrient exchange fluctuations in the area (Lavigne
242 et al. 2015; Macias et al. 2018). To model this process, the spatial mean mixed layer depth
243 (MLD) in the MEDOC area and in a greater polygon around the MEDOC area (MEDOC group,
244 1970), were used as proxies of the vertical extent of winter mixing resulting from open-ocean
245 deep convection in the region (Fig. 1). The MEDOC point (42°N, 5°E) is considered to be the
246 center of convection (Martin et al. 2016).

247 In accordance with the standardised density-based and LPUE-based approaches, annual and
248 monthly estimates of the above environmental variables were obtained and used, respectively
249 (Table 1). For either approach, these variables were examined on 0-, 1- and 2-year lags. The
250 eight environmental variables that were utilized in this study were independent and non-
251 collinear as indicated by the variance inflation factor score ($VIF < 5$) and thus they were
252 examined separately. An influence of AMO on NAO has been documented (Börgel et al. 2020),
253 but here we examined the two indices independently prompted by the variance inflation factor
254 score that we obtained. Regarding chl-a and SST, monthly spatial averages were obtained on a
255 regional scale (i.e. a mean for the whole GSA06 and GSA07) as well as on a local scale for the
256 subareas of Catalan Coast, the Ebro Delta and the Valencia Channel as described above.

257 2.3. Modelling approaches

258 2.3.1 Generalization of empirical orthogonal function (EOF)

259 We seek to estimate one or more modes of spatiotemporal variability in red mullet density and
260 investigate the latent local and nonlocal environmental conditions that may drive this
261 variability. To do so, we employ a statistical generalization of EOF using a spatiotemporal
262 model (Thorson et al. 2020b). Red mullet spatiotemporal density patterns include three
263 components: *i*) temporal variation (β), where the intercept is specified to follow a random-walk
264 and represents fluctuations at all locations from year to year, *ii*) spatial variation (ω) which

265 represents a static long-term spatial pattern, and *iii*) spatiotemporal variation (ε), estimated as
 266 unmeasured variation that is expressed with one or more dominant modes of variability as well
 267 as a map representing the spatial response of density to these estimated modes of variability.
 268 The third component is analogous to “conventional” EOF analysis and generates time series
 269 representing modes (i.e. indices) of variability as well as the associated maps of response.
 270 However, in the present study the spatiotemporal generalization to EOF is estimated after
 271 strictly accounting for expected spatial and temporal components (Thorson et al. 2021).

272 The applied model is a generalized linear mixed model (GLMM) that approximates the
 273 dependent variable of interest using a log link and linear predictors, including Gaussian Markov
 274 random fields representing spatial (ω) and spatiotemporal (ε) variation:

$$275 \quad \text{Log (Density } (s_i, t_i)) = \beta(t_i) + \omega(s_i) + \sum_{f=1}^{N_f} \lambda(t_i, f) \varepsilon(s_i, f) ,$$

276 where, s_i and t_i are, respectively, the location and year associated with sample i whereas N_f is
 277 the number of estimated modes of spatiotemporal variability. Finally, the $\lambda(t_i, f)$ estimate
 278 indicates whether a given year t has a positive phase ($\lambda(t_i, f) > 0$) or a negative phase ($\lambda(t_i, f) < 0$)
 279 during the positive phase of mode f . The $\varepsilon(s_i, f)$ estimate provides the map associated with the
 280 time series $\lambda(t_i, f)$ and represents whether a given location s has a positive or negative value.
 281 The number of modes of spatiotemporal variability was prespecified to 2 ($N_f=2$) in this study
 282 as preliminary sensitivity analyses showed that by increasing their number f , the explanatory
 283 power of the model only increased slightly (Supplementary materials S2).

284 Red mullet density data were fit with a Poisson-link delta-gamma distribution (Thorson 2018),
 285 which is appropriate for zero-inflated biological data where two linear predictors are estimated,
 286 the product of which gives the dependent variable of interest (for further details see Grüss et al.
 287 (2021)). This Poisson-link delta-gamma model specifies a Bernoulli distribution using a
 288 complementary log–log link for encounter/non-encounters (i.e. the probability mass at zero for
 289 a delta-model), and simultaneously specifies that positive catches follow a Gamma distribution
 290 (the probability distribution for non-zeros in a delta-model) (Thorson et al. 2021).

291 Following Thorson et al. (2020a), our modelling approach fixes $\lambda f(t) = 0$ for all $f > t$, with the
292 additional constraint applied in Grüss et al. (2021) that all indices have a sum of zero, i.e.
293 $\sum_{t=0}^{N_t} \lambda(t, f) \varepsilon = 0$, where N_t is the number of years in the time series of interest, such that an
294 “average” year (defined as a hypothetical year t^* when $\sum_{t^*=0}^{N_t} \lambda(t^*, f) = 0$, for all factors) has
295 spatial distribution ω . Then, we rotate the results so that they are directly interpretable as it is
296 commonly done for principal components analysis (PCA) (Zuur et al. 2003a; Thorson et al.
297 2015, 2020a). A rotation matrix P is defined such that ΛP has columns identical to the
298 eigenvectors of $\Lambda^t \Lambda$, and then define ΛP as the factor index and $\Lambda \varepsilon$ as the map associated with
299 it (Thorson et al. 2020a). This “PCA rotation” maximizes the variance for each axis in
300 sequential order (Thorson 2019a; Thorson et al. 2020a).

301 The model parameters were estimated using R package “VAST” (Thorson 2019b) release
302 number 3.10.0, with code and associated materials publicly available online at
303 <https://github.com/James-Thorson-NOAA/VAST>. VAST estimates spatial variables for N_x
304 “knots” for computational efficiency (Shelton et al. 2014) and employs bilinear interpolation
305 to obtain model predictions between knot locations. For both models performed in this study
306 and after carrying out some preliminary sensitivity tests (Supplementary Materials S3), we used
307 $N_x = 100$ knots that were uniformly distributed over the two management units, and predicted
308 response variables across 2500 and 1080 grid cells for GSA06 and GSA07, respectively.

309 After having calculated the annual predicted densities and the static long-term spatial pattern
310 (ω), we computed the 95% quantiles of density in GSA06 and GSA07 and plotted them onto
311 the areas that were consistently characterized by high densities. This was done to further
312 investigate the annual fluctuations of red mullet density, better locate and visualize the areas of
313 high aggregations and, ultimately, examine the environmental variables that may drive these
314 fluctuations (i.e. contraction or expansion of persistent hotspot areas).

315 For each fitted model and to detect environmental processes that may be associated with the
316 spatiotemporal variability in the two areas, we fit an Autoregressive Model (AR) to the first

317 mode of variability in the GSA06 (that explained nearly all variation for GSA06, see section
318 3.1) and the first and second modes of variability in the GSA07. Specifically, a lag-1, AR(1),
319 model was fitted in each case since the modes of variability presented high first-order
320 autocorrelation (not shown). To examine the linkage between the environment and the modes
321 of variability (Grüss et al. 2021), all environmental covariates were incorporated separately in
322 each model. The best model among all models with one environmental covariate was selected
323 based on the Akaike's Information Criterion (AIC). This process was repeated for lag-1 and
324 lag-2 years as well as for those environmental variables that were only available for a subset of
325 the time series examined (Table 1). To test if the annual fluctuations in consistently high-density
326 areas were environmentally driven, we also performed Pearson's correlation tests between
327 environmental variables and the number of cells with an annual density higher than the 95%
328 quantile. If for a given environmental variable, the Pearson's r was high in absolute value
329 (>0.4), it was concluded that this variable has an influence on the mode of variability (Grüss et
330 al. 2021). As the data on chl-a were not available during 1994-1997 (Table 1), to test for
331 significant differences between two r that derived from these different-length datasets, we
332 followed the methodology of (Diedenhofen and Musch 2015) using the "cocor" package they
333 developed. All Pearson's correlations were carried out in lag-0, lag-1 and lag-2 years.

334 2.3.2 Dynamic Factor Analysis (DFA)

335 To identify underlying common trends among LPUE time series and to explore the effects of
336 environmental variables on these long-term trends, a Dynamic Factor Analysis (DFA) was
337 implemented (Zuur et al. 2003b). This is a dimension reduction technique where a set of n
338 observed time series are modelled as a linear combination of m common trends (where $m \ll$
339 n), factor loadings and error terms to explain temporal variability. Factor loadings are used to
340 detect the association between the time series (ports) and the obtained trends. Covariates can
341 optionally be included in the model. DFA is suitable for non-stationary datasets with missing
342 values (Zuur et al. 2003b). The correlation of observation errors can be modelled using different
343 error matrices: (i) same variance and no covariance (diagonal-equal); (ii) different variances

344 and no covariance (diagonal-unequal); (iii) same variance and covariance (equalvarcov); and
345 (iv) different variances and covariances (unconstrained) (Keller et al. 2017; Holmes et al. 2021).
346 The correlations of observation errors were fitted to all possible model structures in the time
347 series, including 1, 2 and 3 common trends.

348 Model selection was based on the standard correction to Akaike's information criterion (AICc)
349 as a measure of goodness-of-fit where the model with the lowest AICc was considered to be
350 the best (Zuur et al. 2003b). Standard errors and confidence intervals of the regression were
351 calculated using the Hessian matrix approach, whereas significance was assessed using a t-test
352 derived from standard errors. DFA was realized in the Multivariate Autoregressive State-Space
353 Modelling (MARSS) package developed for R software (Holmes et al. 2012).

354 In this study, we used monthly time-series data that can be decomposed into seasonal, long-
355 term, and residual variations. The decomposition was realized in base-R with a time-series
356 analysis using the functions "ts" and "decompose". It is thus important to clarify that the
357 seasonal component was removed from the time series since preliminary analyses showed no
358 differentiation in the patterns of LPUE seasonal trends in the GSA06 (Supplementary materials
359 S4). Data were standardized to the mean zero and variance 1 while DFA was applied to an
360 additive combination of long-term and residual components (Holmes et al. 2021).

361 **3. Results**

362 *3.1. Estimating modes of variability*

363 For the Spanish Coast, the first mode of the spatiotemporal variability (ϵ) explained 93.9 % of
364 the total variance and represented a multi-decadal trend (i.e. the values of the mode were
365 positive from 1994 to 2004 and negative thereafter) whereas the second mode explained 6.1%
366 and was characterized by higher interannual variability (Fig. 2). We also generated spatial maps
367 that are associated with each of the two modes of variability on dynamic density hotspots. These
368 areas, which were closely associated with the positive phase of the mode, included the waters
369 off the Catalan Coast and the coastal waters at the South of Valencia Channel. Conversely, two

370 areas in the southern part of the Spanish Coast were highly associated with the negative phase
371 of the mode. Finally, persistent hotspots based on the long-term spatial prediction map (i.e.
372 spatial variation, ω) were also detected with the most prominent found off the Ebro Delta area
373 where the continental shelf is wider.

374 For the Gulf of Lions, the two modes of spatiotemporal variability explained 67.5% and 32.5%
375 of the total variance (Fig 3). The first mode of variability for the Gulf of Lions – as it was the
376 case for the first mode for the Spanish Coast – represents a multi-decadal trend (Fig 3). The
377 areas associated with the positive phase of the first mode were the south-eastern part of the
378 inner Gulf, while a south-eastern extension of the same area was also found to be associated
379 with the positive phase of the second mode of the spatiotemporal variability. The coastal waters
380 in the western limit of the Gulf of Lions were associated with the negative phase of this second
381 mode. The long-term spatial average predicted by the model revealed two persistent hotspots
382 of abundance in the Gulf of Lions, one at the offshore area of the westernmost edge and one at
383 the north-western limit of the wide coastal plain (Fig. 3).

384 The two models predicted the spatial density on an annual basis for the two examined regions
385 where for the Spanish Coast, a high-density area off the Ebro Delta prevails every year with
386 smaller and dynamic high-density areas off the Catalan Coast and at the southern tip of the
387 GSA06 emerging in certain years (Supplementary materials S5). Regarding the Gulf of Lions,
388 the two persistent hotspots identified by the long-term spatial average, appear in every year
389 throughout the time series examined, with lower contribution of the dynamic components in
390 the prediction maps.

391 To assess temporal variation of contraction/expansion over time of persistent high/aggregation
392 areas, we retrieved from the long-term spatial prediction map (i.e. spatial variation, ω) the cells
393 with a density higher than the 95% quantile of total density in the Spanish Coast and the Gulf
394 of Lions and then summarized the number of these cells of the grid as an indicator of the extent
395 of these areas. We show that the red mullet density in the Spanish Coast is steadily high since
396 2012 while the years of 2008 and 2011 exhibit minimal relative density (Fig. 4a, b). Likewise,

397 in the Gulf of Lions, we observe two periods of high density, during 2006-2010 and 2014-2019
398 (Fig 4c, d).

399 *3.2. Links to environmental variables*

400 The first mode of variability for the Spanish Coast was highly related to the Atlantic
401 Multidecadal Oscillation (AMO) on lag-1 and the Mixed Layer Depth in the greater area around
402 MEDOC and the Ebro runoff point on lag-2 years. When considering data only from 1998, no
403 significant relationship with chl-a was identified. For the Gulf of Lions, the first mode was
404 highly associated with the winter SST and the AMO index on lag-0 years. The second mode
405 was associated with the Mixed Layer Depth in MEDOC area on lag-1 years and the Western
406 Mediterranean Oscillation index on lag-2 years (Table 2). No significant effect of chl-a data
407 was detected in models fit in the shorter time series (from 1998 to 2019) for which chl-a data
408 were available. Similar results were obtained with the Pearson's correlation tests when not
409 accounting for first-order autocorrelation (Table S6). It is noteworthy though that more
410 environmental variables were found to be significantly correlated with the modes of variability
411 when applying Pearson's correlations (complementarily and not accounting for autocorrelation)
412 rather than when we fit autoregressive models.

413 With regards to the drivers of contraction/expansion hotspots, Pearson's correlation tests
414 between the size of the persistent areas and environmental variables revealed moderate but
415 significant links ($p < 0.05$) between the density in the Spanish Coast and the WeMOi and NAO
416 lag-1 indices. Interestingly, the highest correlation for the Spanish Coast was detected to be
417 with the lag-0 winter SST of the Gulf of Lions ($r = 0.57$, $p < 0.05$). Finally, the only variable that
418 was found to be associated with the annual variations of density in the Gulf of Lions was the
419 lag-1 AMO index ($r = 0.43$, $p < 0.05$). Besides the four aforementioned drivers, all remaining
420 environmental variables presented no significant correlations.

421 3.3. DFA on LPUE data

422 After we had examined all possible model structures regarding the number of trends and the
423 variance and the error matrices, we found that the best fit for the long-term trends of LPUE
424 included models with three trends ($m=3$) (Fig. 5a) and an unconstrained matrix (different
425 variance and covariance) (Table 3). The incorporation of any of the environmental variables
426 did not improve the model (not shown). The first trend exhibits a steep increase in LPUE from
427 2006 peaking in 2008, followed by a 10-year period of relatively low fluctuations that ended
428 with a decline in 2018. Ports around Ebro Delta were associated with the first trend for which
429 they presented negative factor loadings (Fig. 5b). The second trend reveals a steady upward
430 tendency in LPUE starting from 2008 while the third trend shows a decline from 2005 until
431 2010 that is followed by a relatively constant period of low LPUE that ended in 2015 with a
432 slow increase (Fig 5b). Ports along the Catalan Coast were associated with the second and third
433 trends and presented substantial variability with negative and positive factor loadings for either
434 of the trends. Finally, the four southernmost landing ports in our study area, south of the
435 Valencia Channel, were associated with the first and the second trends, with negative and
436 positive factor loadings, respectively (Fig. 5b). A preliminary analysis on the seasonal and
437 residual variation showed no differentiation in the seasonal trends of LPUE across the Spanish
438 Coast.

439 4. Discussion

440 In this study, we examined spatiotemporal variation in the distributions and densities of a
441 commercially important species to identify environmental drivers of population structure and
442 assess the potential utility of implementing a spatially explicit stock assessment. We detected
443 persistent and dynamic aggregations of a red mullet population from fisheries-independent data
444 and explored whether these aggregations are linked to spatial patterns derived from fisheries-
445 dependent data of landings in the NW Mediterranean Sea. To do so, we applied a combination
446 of a generalized EOF analysis (Thorson et al. 2020a; Grüss et al. 2021) and a DFA (Zuur et al.

447 2003b) to complement fine spatiotemporal variation at annual scale with seasonal dynamics
448 along the geographic gradient. Our study also informs on the effect of latent environmental
449 processes on the spatial biocomplexity of the red mullet population system in the NW
450 Mediterranean Sea. The NW Mediterranean open-ocean convection was shown to influence the
451 dynamics of both management units considered in this study, GSA06 and GSA07. Model
452 predictions indicated that red mullet populations along the Spanish coast were equally
453 characterized by dynamic and persistent aggregations whereas those in the Gulf of Lions
454 primarily consisted of persistent aggregations. Regarding landings data, three trends were
455 detected in the long-term monthly LPUE of the Spanish Coast with a primary segregation of
456 the ports that were closely related to the persistent population unit off the Ebro Delta.

457 Identifying persistent areas of high density for marine organisms is of paramount importance
458 for conservation and management as these could be candidate areas for the implementation of
459 specific measures such as spatiotemporal closures through the detection of essential fish
460 habitats (STECF 2022) or the designation of marine protected areas (MPAs) (Agardy 2000;
461 Erisman et al. 2017). In the Spanish Coast, we found that the continental shelf off the Ebro
462 Delta is the main high-density and high-persistence area for the red mullet, which is consistent
463 with previous studies (e.g. Paradinas et al. 2020). Discharges from the Ebro River and the
464 prevailing Northern current jointly increase the primary productivity around the Delta area
465 (Estrada 1996), which could then favour the productivity in higher trophic levels (Donoso et al.
466 2017). Since Coll et al. (2016) pointed out that the greater Ebro Delta is an important biomass
467 area for different species, recent studies evidenced that this area is of central importance for a
468 variety of demersal resources of the NW Mediterranean (Vilas et al. 2020; Paradinas et al.
469 2022), including the red mullet (Paradinas et al. 2020). As such, Ebro Delta may be viewed as
470 a demographic engine for the regional persistence and population dynamics in the Western
471 Mediterranean (Kerametsidis et al. 2023). In the Gulf of Lions, by contrast, two areas with
472 persistent aggregations of red mullet were identified. The Gulf as a whole is indeed one of the
473 most productive areas of the entire Mediterranean Sea due to complex coupled ocean-

474 atmosphere processes (Millot 1990; Bosc et al. 2004). One of the two persistent high-density
475 areas was located on the continental shelf off the westernmost part of the gulf (Fig. 3) which is
476 consistent with the very high densities of red mullet reported by (Morfin et al. 2016). The
477 second persistent area is located in the eastern part of the Inner Gulf and could also be related
478 to the Rhône River discharges (Vandenbulcke and Barth 2019), a prominent hydrographical
479 feature that greatly affects productivity in the area (Ulses 2008) similar to Ebro River in the
480 Spanish Coast.

481 We identified dynamic high-density areas in both management units which are equally
482 important as the persistent ones that were described above. These areas can also be used to
483 explore the link between environmental and biological components of the ecosystem. A notable
484 result of our study that holds true for both examined management units was the high correlation
485 detected between the spatiotemporal variability of red mullet density and the NW
486 Mediterranean open-ocean convection. Despite the latter being a very influential oceanographic
487 phenomenon in the Western Mediterranean, greatly affecting primary productivity
488 (Heimbürger-Boavida et al. 2013), zooplankton communities (Donoso et al. 2017) and even
489 small-pelagic stocks (Feuilloley et al. 2020), its relation to demersal fish stock dynamics has to
490 date only been demonstrated for two species in the area, hake and blue whiting (Massutí et al.
491 2008; Martín et al. 2012; Hidalgo et al. 2019a). Since deep convection strongly drives
492 zooplankton dynamics, which represent a large portion of red mullet diet over different
493 ontogenetic stages (Bautista-Vega et al. 2008; Esposito et al. 2014), it is not surprising that we
494 detected significant correlations between convective events and red mullet density in both
495 management units. In addition, NW Mediterranean open-ocean convection events dramatically
496 affect primary productivity dynamics in the region (Estrada 1996; Sabatés et al. 2015). Sabatés
497 et al. (2015) maintained that chl-*a* concentrations are indirectly associated with the distribution
498 and feeding dynamics of red mullet larvae mediated via the fluctuations of one of its main
499 preys, the cladocera. This is in line with our findings regarding the critical effect of open-ocean
500 convection.

501 The Atlantic Multidecadal Oscillation has been shown to play an important role in demersal
502 fish and invertebrate communities (Nye et al. 2014; Zimmermann et al. 2019). In the
503 Mediterranean Sea, small pelagic fish communities (Tsikliras et al. 2019) have also been
504 associated with AMO, with the western basin being particularly affected. Our results suggest
505 that AMO played a significant role in shaping red mullet dynamics across a wide geographical
506 gradient in the NW Mediterranean Sea. Notably, AMO emerged as the predominant process
507 affecting the extent of persistently high-density areas in the Gulf of Lions. Furthermore, another
508 regional climatic index, the WeMO index, was associated with the spatiotemporal variability
509 of red mullet in the Gulf of Lions. To our knowledge, this is the first study to document an
510 effect of this process on the red mullet although the effect of WeMO on another important
511 demersal species, the hake, has been previously documented in the Spanish Coast (Martín et al.
512 2012; Ordines et al. 2019). The relationship between red mullet density variations and two
513 broad-scale coupled atmosphere-ocean climatic indices documented here underlines the utility
514 of such synthesized indices to assess population dynamics on local scales as, in certain cases,
515 they can be better tools to predict ecological processes than are local environmental variables
516 (Hallett et al. 2004; Stenseth and Mysterud 2005). However, we must acknowledge that the
517 first modes of variability for both areas display long-term trends and low-frequency cycles that
518 could also be due to the recruitment spread among age classes, generating autocovariance
519 between cohorts (Fromentin and Fonteneau 2001) and inter- or intra-cohort interactions
520 (Bjørnstad et al. 1999). Also, the periods of climatic oscillations (e.g. >50 yr for AMO) are
521 often larger than the information available. These factors often limit the mechanistic
522 understanding between climatic indices and ecological response.

523 Our study also revealed the influence of other local environmental drivers. SST is a variable
524 that is routinely used as an environmental driver for stock dynamics as it affects fish directly
525 (e.g. via positive relationships with physiological processes such as metabolism) and indirectly
526 (e.g. via fluctuations in prey availability) (Lloret et al. 2014; Brosset et al. 2015). Here, we
527 found that winter SST is the primary driver of red mullet dynamics in the Gulf of Lions. This

528 is in accordance with Kerametsidis et al. (2023) who documented that higher winter SST
529 favours the recruitment success of red mullet in the Western Mediterranean. Furthermore, Levi
530 et al. (2003) showed that SST anomalies significantly influence red mullet in the Central
531 Mediterranean Sea. The density and biomass of demersal communities in the NW
532 Mediterranean have been previously shown to be positively impacted by higher SST (Vilas et
533 al. 2020).

534 The monthly LPUE data from commercial fisheries allowed concluding that the intra-annual
535 dynamics of the species and the supporting fishery is consistent with the spatial structure and
536 dynamics of the sub-units identified here. The DFA performed on LPUE from ports along the
537 Northern Spanish Coast revealed that the long-term variability can be explained by three
538 underlying trends. No environmental influence on either of the trends was detected as none of
539 the examined environmental processes improved the performance of the model. Since DFA
540 was performed in fishery-dependent data, it is very likely that other non-environmental (e.g.
541 socio-economic factors), such as market-related variables, or intrinsic stock characteristics may
542 determine such trends (Bjørnstad et al. 1999; Aguilera et al. 2015). These trends show that the
543 ports around the Ebro Delta were clustered together, separately from the remainders in the
544 Catalan coast and the south of Valencia Channel. This once again underlines the importance of
545 Ebro Delta for red mullet and its partially independent dynamics. This is also in accordance
546 with EOFs that identified the area off Ebro Delta as a persistent hotspot for red mullet density
547 as well as for a variety of other species as previously explained.

548 Non-environmental variables were not included in this study as our primary objective was to
549 identify the environmental components that drive the density variability of red mullet in the
550 NW Mediterranean Sea across different scales. Although red mullet has constantly been
551 harvested unsustainably (Colloca et al. 2017), obtaining reliable information on fishing
552 mortality on a local level (i.e. inferior to the management unit level) proved challenging, so we
553 opted not to incorporate this information into our study. Additionally, we refrained from
554 including habitat degradation as this has been shown to be relevant to organisms of meiobenthos

555 and superbenthos (Coll et al. 2010). These, in addition to other variables such as pollution,
556 trophic interactions etc. could be explored in future cross-scale studies and/or under various
557 climate change scenarios. This would be particularly important for the trends of LPUE data
558 which seemed not to be related to any of the candidate environmental drivers that we explored.

559 **Conclusion, broad implications, and future research**

560 Here we demonstrate the existence of both persistent and dynamic high-density areas for a well-
561 studied high-value species across two adjacent management units of the western Mediterranean
562 Sea. Persistent dynamic aggregations were associated with different environmental drivers that
563 varied by spatial scale and temporal dynamics. This shows that the population of the species in
564 the examined region is spatially segregated among and within the two management units. This
565 suggests a metapopulation structure for this species in the area (Cadrin and Dickey-Collas
566 2014) , which should reasonably be considered in its assessment. Additional studies applying
567 other stock identification techniques could provide conclusive evidence on the dynamics of
568 such metapopulation structure and on the (bi)directional connections among the sub-units.
569 Thus, the combination of various tools (i.e. generalized EOF and DFA) applied on
570 complementary datasets (i.e. CPUE, LPUE) to explore and quantify demographic connectivity
571 at both local and regional scales is strongly encouraged for future studies. Some of these
572 techniques might include tagging, analyses of otolith shape and microchemistry, white muscle
573 stable isotope analysis, morphometrics or population dynamics simulations assuming complex
574 population structures (Goethel et al. 2011, 2021, ICES 2022). This study is the first to non-
575 gadoid species, supporting a possible generalization of the impacts of open-ocean convective
576 events on the local and/or regional population dynamics in the Mediterranean Sea. Taking into
577 account that convective events outside the Mediterranean Sea have been associated directly and
578 indirectly to salinity and primary productivity variations (e.g. Ferrari et al. 2015; Chan et al.
579 2017; Lowry et al. 2018)), it could be of elevated importance to investigate the link between
580 open-ocean convection and stock dynamics in areas with considerable convective events such
581 as Greenland and Labrador Seas (Marshall and Schott 1999).

582 As we revealed persistent high-density areas, our findings could be used as a basis for the
583 development of area-based fisheries management measures. Area-based management schemes
584 can help achieve maximum sustainable yield (MSY) and maximize socio-economic benefits
585 over the long term for the fishers (STECF 2022), and they are regarded as an effective
586 framework to achieve sustainability of marine resources. In our case study, for instance, one of
587 the persistent areas that was identified for red mullet is Ebro Delta, an area that has been
588 highlighted as important for other exploited demersal species already (Vilas et al. 2020). It is
589 noteworthy that time closures, as an area-based measure, have recently been enforced within
590 the Ebro Delta area (STECF 2021). In addition, understanding the spatial structure of marine
591 stocks is vital for effective management. The segregation of different subpopulations within the
592 same management unit indicates that the implementation of spatial stock assessment
593 frameworks (Goethel et al. 2011, 2023; Punt 2019) might be more suitable to inform the
594 management of red mullet stock in the region. Finally, this study shows that besides spatial
595 biocomplexity in marine stocks, it is equally crucial that other ecosystem components, such as
596 environmental processes, be integrated into assessment frameworks in the context of EBFM.

597 **Acknowledgments**

598 We thank all the dedicated people of the Instituto Español de Oceanografía (IEO, Spain), who
599 have worked on the research vessels and MEDITS surveys. Additionally, we would like to
600 thank Dr Patricia Puerta for her insightful comments during the implementation of DFA.
601 Finally, we thank the anonymous reviewers for their careful reading of our manuscript and their
602 highly useful remarks and suggestions.

603 **Funding**

604 MEDITS surveys are funded by IEO and the European Union (EU) through the European
605 Maritime and Fisheries Fund (EMFF) within the National Program of collection, management
606 and use of data in the fisheries sector and support for scientific advice regarding the Common
607 Fisheries Policy. GK, AE, EG, MV and MH acknowledge funding from the COCOCHA project

608 (Grant PID2019-110282RA-I00 funded by MCIN/AEI/ 10.13039/501100011033). GK
609 acknowledges funding from the Grant for PhD candidates (FPI) PRE2020-094321 funded by
610 MCIN/AEI/ 10.13039/501100011033 by the “European Union NextGenerationEU/PRTR” and
611 co-funded by the European Social Fund.

612 **Author contributions**

613 Conceptualization: MH; Methodology: GK, JT, CB and MH; Validation: GK, JT, CB and MH;
614 Formal analysis: GK, JT, CB and MH; Investigation: GK, MH; Resources & Data Curation:
615 GK, JT, VR, DAB, CB, GC, AE, EG, AJ, SP, MV and MH; Writing-original draft preparation:
616 GK, MH; Writing-review and editing: GK, JT, VR, DAB, CB, GC, AE, EG, AJ, SP, MV and
617 MH; Visualization: GK, JT, GC, CB, MH; Supervision: MH; Project administration: GK, MH;
618 Funding acquisition: GK, AE, EG, MV and MH. All authors have read and agreed to the
619 submitted version of the manuscript.

620 **Declaration of competing interest**

621 The authors declare that they have no known competing financial interests or personal
622 relationships that could have appeared to influence the work reported in this paper.

623 **Data availability**

624 The data analyzed during this study are available from the corresponding author upon
625 reasonable request.

626 **References**

- 627 Agardy, T., 2000. Information needs for marine protected areas: scientific and societal.
628 *Bulletin of Marine Science*, 66: 875-888
- 629 Aguilera, S.E., Cole, J., Finkbeiner, E.M., Le Cornu, E., Ban, N.C., Carr, M.H., Cinner, J.E.,
630 Crowder, L.B., Gelcich, S., Hicks, C.C., Kittinger, J.N., Martone, R., Malone, D.,
631 Pomeroy, C., Starr, R.M., Seram, S., Zuercher, R., and Broad, K. 2015. Managing
632 small-scale commercial fisheries for adaptive capacity: Insights from dynamic social-
633 ecological drivers of change in monterey bay. *PLoS One* **10**(3). Public Library of
634 Science. doi:10.1371/journal.pone.0118992.

- 635 Anonymous (2017) “MEDITS-Handbook. Version n. 9, 2017, MEDITS Working
636 Group : 106 pp.”
- 637 Bautista-Vega, A.A., Letourneur, Y., Harmelin-Vivien, M., and Salen-Picard, C. 2008.
638 Difference in diet and size-related trophic level in two sympatric fish species, the red
639 mullets *Mullus barbatus* and *Mullus surmuletus*, in the Gulf of Lions (north-west
640 Mediterranean Sea). *J Fish Biol* **73**(10): 2402–2420. doi:10.1111/j.1095-
641 8649.2008.02093.x.
- 642 Bjørnstad, O.N., Ims, R.A., and Lambin, X. 1999. Spatial population dynamics: analyzing
643 patterns and processes of population synchrony. *Trends in Ecology & Evolution*, 14(11),
644 pp.427-432.
- 645 Börgel, F., Frauen, C., Neumann, T., and Meier, H.E.M. 2020. The Atlantic Multidecadal
646 Oscillation controls the impact of the North Atlantic Oscillation on North European
647 climate. *Environmental Research Letters* **15**(10). IOP Publishing Ltd. doi:10.1088/1748-
648 9326/aba925.
- 649 Bosc, E., Bricaud, A., and Antoine, D. 2004. Seasonal and interannual variability in algal
650 biomass and primary production in the Mediterranean Sea, as derived from 4 years of
651 SeaWiFS observations. *Global Biogeochem Cycles* **18**(1). American Geophysical
652 Union. doi:10.1029/2003gb002034.
- 653 Bowler, D.E., Hof, C., Haase, P., Kröncke, I., Schweiger, O., Adrian, R., Baert, L., Bauer,
654 H.G., Blick, T., Brooker, R.W., Dekoninck, W., Domisch, S., Eckmann, R., Hendrickx,
655 F., Hickler, T., Klotz, S., Kraberg, A., Kühn, I., Matesanz, S., Meschede, A., Neumann,
656 H., O’Hara, R., Russell, D.J., Sell, A.F., Sonnewald, M., Stoll, S., Sundermann, A.,
657 Tackenberg, O., Türkay, M., Valladares, F., Van Herk, K., Van Klink, R., Vermeulen,
658 R., Voigtländer, K., Wagner, R., Welk, E., Wiemers, M., Wiltshire, K.H., and Böhning-
659 Gaese, K. 2017. Cross-realm assessment of climate change impacts on species’
660 abundance trends. *Nat Ecol Evol* **1**(3). Nature Publishing Group. doi:10.1038/s41559-
661 016-0067.
- 662 Brosset, P., Ménard, F., Fromentin, J.M., Bonhommeau, S., Ulses, C., Bourdeix, J.H., Bigot,
663 J.L., Van Beveren, E., Roos, D., and Saraux, C. 2015. Influence of environmental
664 variability and age on the body condition of small pelagic fish in the Gulf of Lions. *Mar*
665 *Ecol Prog Ser* **529**: 219–231. Inter-Research. doi:10.3354/meps11275.
- 666 Cadrin, S.X. 2020. Defining spatial structure for fishery stock assessment. *Fish Res* **221**.
667 Elsevier B.V. doi:10.1016/j.fishres.2019.105397.
- 668 Cadrin, S.X., and Dickey-Collas, M. 2014. Stock assessment methods for sustainable
669 fisheries. *In* *ICES Journal of Marine Science*. Oxford University Press. pp. 1–6.
670 doi:10.1093/icesjms/fsu228.
- 671 Cardinale, M., Colloca, F., Bonanno, A., Scarcella, G., Arneri, E., Jadaud, A., Saraux, C.,
672 Aronica, S., Genovese, S., Barra, M., Basilone, G., Angelini, S., Falsone, F., Gancitano,
673 V., Santojanni, A., Fiorentino, F., Milisenda, G., Murenu, M., Russo, T., Carpi, P.,
674 Guijarro, B., Gil, J.L.P., González, M., Torres, P., Giráldez, A., García, C., Esteban, A.,
675 García, E., Vivas, M., Massutí, E., Ordines, F., Quetglas, A., and Herrera, J.G. 2021.
676 The Mediterranean fishery management: A call for shifting the current paradigm from
677 duplication to synergy. *Mar Policy* **131**. Elsevier Ltd.
678 doi:10.1016/j.marpol.2021.104612.

- 679 Champion, C., Brodie, S., and Coleman, M.A. 2021. Climate-Driven Range Shifts Are Rapid
680 Yet Variable Among Recreationally Important Coastal-Pelagic Fishes. *Front Mar Sci* **8**.
681 *Frontiers Media S.A.* doi:10.3389/fmars.2021.622299.
- 682 Chan, P., Halfar, J., Adey, W., Hetzinger, S., Zack, T., Moore, G.W.K., Wortmann, U.G.,
683 Williams, B., and Hou, A. 2017. Multicentennial record of Labrador Sea primary
684 productivity and sea-ice variability archived in coralline algal barium. *Nat Commun* **8**.
685 *Nature Publishing Group.* doi:10.1038/ncomms15543.
- 686 Clark, M., Macdiarmid, J., Jones, A.D., Ranganathan, J., Herrero, M., and Fanzo, J. 2020. The
687 Role of Healthy Diets in Environmentally Sustainable Food Systems. *Food Nutr Bull*
688 **41**(2_suppl): 31S-58S. *SAGE Publications Inc.* doi:10.1177/0379572120953734.
- 689 Coll, M., Piroddi, C., Steenbeek, J., Kaschner, K., Lasram, F.B.R., Aguzzi, J., Ballesteros, E.,
690 Bianchi, C.N., Corbera, J., Dailianis, T., Danovaro, R., Estrada, M., Froggia, C., Galil,
691 B.S., Gasol, J.M., Gertwage, R., Gil, J., Guilhaumon, F., Kesner-Reyes, K., Kitsos,
692 M.S., Koukouras, A., Lampadariou, N., Laxamana, E., de la Cuadra, C.M.L.F., Lotze,
693 H.K., Martin, D., Mouillot, D., Oro, D., Raicevich, S., Rius-Barile, J., Saiz-Salinas, J.I.,
694 Vicente, C.S., Somot, S., Templado, J., Turon, X., Vafidis, D., Villanueva, R., and
695 Voultsiadou, E. 2010. The biodiversity of the Mediterranean Sea: Estimates, patterns,
696 and threats. doi:10.1371/journal.pone.0011842.
- 697 Coll, M., Steenbeek, J., Sole, J., Palomera, I., and Christensen, V. 2016. Modelling the
698 cumulative spatial-temporal effects of environmental drivers and fishing in a NW
699 Mediterranean marine ecosystem. *Ecol Modell* **331**: 100–114. *Elsevier B.V.*
700 doi:10.1016/j.ecolmodel.2016.03.020.
- 701 Colloca, F., Scarcella, G., and Libralato, S. 2017, August 14. Recent trends and impacts of
702 fisheries exploitation on Mediterranean stocks and ecosystems. *Frontiers Media S. A.*
703 doi:10.3389/fmars.2017.00244.
- 704 Diedenhofen, B., and Musch, J. 2015. Cocor: A comprehensive solution for the statistical
705 comparison of correlations. *PLoS One* **10**(4). *Public Library of Science.*
706 doi:10.1371/journal.pone.0121945.
- 707 Dijkstra, H.A., Te Raa, L., Schmeits, M., and Gerrits, J. 2006. On the physics of the Atlantic
708 Multidecadal Oscillation. *Ocean Dyn* **56**(1): 36–50. doi:10.1007/s10236-005-0043-0.
- 709 Donoso, K., Carlotti, F., Pagano, M., Hunt, B.P.V., Escribano, R., and Berline, L. 2017.
710 Zooplankton community response to the winter 2013 deep convection process in the
711 NW Mediterranean Sea. *J Geophys Res Oceans* **122**(3): 2319–2338. *Blackwell*
712 *Publishing Ltd.* doi:10.1002/2016JC012176.
- 713 Erisman, B., Heyman, W., Kobara, S., Ezer, T., Pittman, S., Aburto-Oropeza, O., and
714 Nemeth, R.S. 2017. Fish spawning aggregations: where well-placed management
715 actions can yield big benefits for fisheries and conservation. *Fish and Fisheries* **18**(1):
716 128–144. *Blackwell Publishing Ltd.* doi:10.1111/faf.12132.
- 717 Esposito, V., Andaloro, F., Bianca, D., Natalotto, A., Romeo, T., Scotti, G., and Castriota, L.
718 2014. Diet and prey selectivity of the red mullet, *Mullus barbatus* (Pisces: Mullidae),
719 from the southern Tyrrhenian Sea: The role of the surf zone as a feeding ground. *Marine*
720 *Biology Research* **10**(2): 167–178. doi:10.1080/17451000.2013.797585.
- 721 Estrada, M. 1996. Primary production in the northwestern Mediterranean. *In* THE
722 EUROPEAN ANCHOVY AND ITS ENVIRONMENT.

- 723 Ferrari, R., Merrifield, S.T., and Taylor, J.R. 2015. Shutdown of convection triggers increase
724 of surface chlorophyll. *Journal of Marine Systems* **147**: 116–122. Elsevier.
725 doi:10.1016/j.jmarsys.2014.02.009.
- 726 FAO. 2022a. The State of World Fisheries and Aquaculture 2022. Towards Blue
727 Transformation. Rome, FAO. <https://doi.org/10.4060/cc0461en>
- 728 FAO. 2022b. The State of Mediterranean and Black Sea Fisheries 2022. General Fisheries
729 Commission for the Mediterranean. Rome. <https://doi.org/10.4060/cc3370en>
- 730 Feuilleley, G., Fromentin, J.-M., Stemmann, L., Demarcq, H., Estournel, C., and Sarau, C.
731 2020. Concomitant changes in the Environment and small pelagic fish community of the
732 Gulf of Lions. *Progress in Oceanography*, 186, p.102375.
- 733 Fiorentino F., E. Massutì, F. Tinti, S. Somarakis, G. Garofalo, T. Russo, M.T. Facchini,
734 P. Carbonara, K. Kapiris, P. Tugores, R. Cannas, C. Tsigenopoulos, B. Patti, F. Colloca,
735 M. Sbrana, R. Mifsud, V. Valavanis, and M.T. Spedicato, 2015. Stock units:
736 Identification of distinct biological units (stock units) for different fish and shellfish
737 species and among different GFCM-GSA. STOCKMED Deliverable 03: FINAL
738 REPORT. January 2015, 310 p
- 739 Fischer W., Bauchot M.L., Schneider M. 1987. Fiches FAO d'identification des espèces pour
740 les besoins de la pêche. (Révision 1). Méditerranée et Mer Noire. Zone de pêche 37. 2.
741 Vertébrés. Publication préparée par la FAO (Project GCP/INT/422/EEC). Rome, FAO:
742 761-1530.
- 743 Gargano, F., Garofalo, G., and Fiorentino, F. 2017. Exploring connectivity between spawning
744 and nursery areas of *Mullus barbatus* (L., 1758) in the Mediterranean through a dispersal
745 model. *Fish Oceanogr* **26**(4): 476–497. Blackwell Publishing Ltd.
746 doi:10.1111/fog.12210.
- 747 Gargano, F., Garofalo, G., Quattrocchi, F., and Fiorentino, F. 2022. Where do recruits come
748 from? Backward Lagrangian simulation for the deep water rose shrimps in the Central
749 Mediterranean Sea. *Fish Oceanogr* **31**(4): 369–383. John Wiley and Sons Inc.
750 doi:10.1111/fog.12582.
- 751 Goethel, D.R., and Berger, A.M. 2016. Accounting for spatial complexities in the calculation
752 of biological reference points: Effects of misdiagnosing population structure for stock
753 status indicators. *Canadian Journal of Fisheries and Aquatic Sciences* **74**(11): 1878–
754 1894. Canadian Science Publishing. doi:10.1139/cjfas-2016-0290.
- 755 Goethel, D.R., Berger, A.M., and Cadrin, S.X. 2023. Spatial awareness: Good practices and
756 pragmatic recommendations for developing spatially structured stock assessments. *Fish*
757 *Res* **264**. Elsevier B.V. doi:10.1016/j.fishres.2023.106703.
- 758 Goethel, D.R., Bosley, K.M., Langseth, B.J., Deroba, J.J., Berger, A.M., Hanselman, D.H.,
759 and Schueller, A.M. 2021. Where do you think you're going? Accounting for
760 ontogenetic and climate-induced movement in spatially stratified integrated population
761 assessment models. *Fish and Fisheries* **22**(1): 141–160. Blackwell Publishing Ltd.
762 doi:10.1111/faf.12510.
- 763 Goethel, D.R., Quinn, T.J., and Cadrin, S.X. 2011. Incorporating spatial structure in stock
764 assessment: Movement modeling in marine fish population dynamics. *Reviews in*
765 *Fisheries Science* **19**(2): 119–136. Taylor and Francis Inc.
766 doi:10.1080/10641262.2011.557451.

- 767 Grüss, A., Thorson, J.T., Stawitz, C.C., Reum, J.C.P., Rohan, S.K., and Barnes, C.L. 2021.
768 Synthesis of interannual variability in spatial demographic processes supports the strong
769 influence of cold-pool extent on eastern Bering Sea walleye pollock (*Gadus*
770 *chalcogrammus*). *Prog Oceanogr* **194**. Elsevier Ltd. doi:10.1016/j.pocean.2021.102569.
- 771 Hallett, T. B., Coulson, T., Pilkington, J. G., Clutton-Brock, T. H., Pemberton, J. M., &
772 Grenfell, B. T. 2004. Why large-scale climate indices seem to predict ecological
773 processes better than local weather. *Nature*, 430(6995), 71-75.
- 774 Heimbürger-Boavida, L.-E., Lavigne, H., Migon, C., Estournel, C., Coppola, L., Miquel, J.-
775 C., Es-, C., and Heimbürger, L.-E. (2013). Temporal variability of vertical export flux at
776 the DYFAMED time-series station (Northwestern Mediterranean Sea).
777 doi:10.1016/j.pocean.2013.08.005i.
- 778 Hidalgo, M., Rossi, V., Monroy, P., Ser-Giacomi, E., Hernández-García, E., Guijarro, B.,
779 Massutí, E., Alemany, F., Jadaud, A., Perez, J.L., and Reglero, P. 2019a. Accounting for
780 ocean connectivity and hydroclimate in fish recruitment fluctuations within
781 transboundary metapopulations. *Ecological Applications* **29**(5). Ecological Society of
782 America. doi:10.1002/eap.1913.
- 783 Hidalgo, M., Ligas, A., Bellido, J.M., Bitetto, I., Carbonara, P., Carlucci, R., Guijarro, B.,
784 Jadaud, A., Lembo, G., Manfredi, C., Esteban, A., Garofalo, G., Ikica, Z., García, C., de
785 Sola, L.G., Kavadas, S., Maina, I., Sion, L., Vittori, S., and Vrgoc, N. 2019b. Size-
786 dependent survival of european hake juveniles in the Mediterranean sea. *Sci Mar*
787 **83**(S1): 207–221. CSIC Consejo Superior de Investigaciones Cientificas.
788 doi:10.3989/scimar.04857.16A.
- 789 Hiddink, J.G., and ter Hofstede, R. 2008. Climate induced increases in species richness of
790 marine fishes. *Glob Chang Biol* **14**(3): 453–460. doi:10.1111/j.1365-
791 2486.2007.01518.x.
- 792 Holmes, E., Villanueva, N.M., Sestelo, M., and Zhang, W. 2012. MARSS: multivariate
793 autoregressive state-space models for analyzing time-series data. *R J.*, 4(1), p.11.
- 794 Holmes, Elizabeth Eli, Ward, Eric J., Scheuerell, Mark D., Wills K. 2021. MARSS:
795 Multivariate Autoregressive State-Space Modeling. R package version 3.11.4.
796 <https://CRAN.R-project.org/package=MARSS>
- 797 Houde, E.D. 2016. Recruitment Variability. *Fish reproductive biology: implications for*
798 *assessment and management*, pp.98-187.
- 799 Houpert, L., Durrieu de Madron, X., Testor, P., Bosse, A., D'Ortenzio, F., Bouin, M.N.,
800 Dausse, D., Le Goff, H., Kunesch, S., Labaste, M., Coppola, L., Mortier, L., and
801 Raimbault, P. 2016. Observations of open-ocean deep convection in the northwestern
802 Mediterranean Sea: Seasonal and interannual variability of mixing and deep water
803 masses for the 2007-2013 Period. *J Geophys Res Oceans* **121**(11): 8139–8171.
804 Blackwell Publishing Ltd. doi:10.1002/2016JC011857.
- 805 ICES. 2022. Stock Identification Methods Working Group (SIMWG). ICES Scientific
806 Reports. 4:72. 66 pp. <http://doi.org/10.17895/ices.pub.20937001>
- 807 Kerametsidis, G., Rueda, L., Bellido, J.M., Esteban, A., García, E., Gil de Sola, L., Pennino,
808 M.G., Pérez-Gil, J.L., and Hidalgo, M. 2023. The trade-off between condition and
809 growth shapes juveniles' survival of harvested demersal fish of the Mediterranean sea.
810 *Mar Environ Res* **184**. Elsevier Ltd. doi:10.1016/j.marenvres.2022.105844.

- 811 Keller, S., Quetglas, A., Puerta, P., Bitetto, I., Casciaro, L., Cuccu, D., Esteban, A., Garcia,
812 C., Garofalo, G., Guijarro, B., Josephides, M., Jadaud, A., Lefkaditou, E., Maiorano, P.,
813 Manfredi, C., Marceta, B., Micallef, R., Peristeraki, P., Relini, G., Sartor, P., Spedicato,
814 M.T., Tserpes, G., and Hidalgo, M. 2017. Environmentally driven synchronies of
815 Mediterranean cephalopod populations. *Prog Oceanogr* **152**: 1–14. Elsevier Ltd.
816 doi:10.1016/j.pocean.2016.12.010.
- 817 Kerr, L.A., Hintzen, N.T., Cadrin, S.X., Clausen, L.W., Dickey-Collas, M., Goethel, D.R.,
818 Hatfield, E.M.C., Kritzer, J.P., and Nash, R.D.M. 2017, July 1. Lessons learned from
819 practical approaches to reconcile mismatches between biological population structure
820 and stock units of marine fish. Oxford University Press. doi:10.1093/icesjms/fsw188.
- 821 Knight, J.R., Folland, C.K., and Scaife, A.A. 2006. Climate impacts of the Atlantic
822 multidecadal oscillation. *Geophys Res Lett* **33**(17). American Geophysical Union.
823 doi:10.1029/2006GL026242.
- 824 Lavigne, H., D'Ortenzio, F., Ribera D'Alcalà, M., Claustre, H., Sauzède, R., and Gacic, M.
825 2015. On the vertical distribution of the chlorophyll a concentration in the
826 Mediterranean Sea: A basin-scale and seasonal approach. *Biogeosciences* **12**(16): 5021–
827 5039. Copernicus GmbH. doi:10.5194/bg-12-5021-2015.
- 828 Levi, D., Andreoli, M.G., Bonanno, A., Fiorentino, F., Garofalo, G., Mazzola, S., Norrito, G.,
829 Patti, B., Pernice, G., Ragonese, S., Giusto, G.B., Rizzo, P., 2003. Embedding sea
830 surface temperature anomalies into the stock recruitment relationship of red mullet
831 (*Mullus barbatus* L. 1758) in the Strait of Sicily. *Sci. Mar.* **67**, 259–268.
832 <https://doi.org/10.3989/scimar.2003.67s1259>.
- 833 Lloret, J., Shulman, G., Love, R.M., 2014. Condition and Health Indicators of Exploited
834 Marine Fishes, vol. 263.
- 835 Lotze, H.K., Tittensor, D.P., Bryndum-Buchholz, A., Eddy, T.D., Cheung, W.W.L.,
836 Galbraith, E.D., Barange, M., Barrier, N., Bianchi, D., Blanchard, J.L., Bopp, L.,
837 Büchner, M., Bulman, C.M., Carozza, D.A., Christensen, V., Coll, M., Dunne, J.P.,
838 Fulton, E.A., Jennings, S., Jones, M.C., Mackinson, S., Maury, O., Niiranen, S.,
839 Oliveros-Ramos, R., Roy, T., Fernandes, J.A., Schewe, J., Shin, Y.J., Silva, T.A.M.,
840 Steenbeek, J., Stock, C.A., Verley, P., Volkholz, J., Walker, N.D., and Worm, B. 2019.
841 Global ensemble projections reveal trophic amplification of ocean biomass declines with
842 climate change. *Proc Natl Acad Sci U S A* **116**(26): 12907–12912. National Academy of
843 Sciences. doi:10.1073/pnas.1900194116.
- 844 Lowry, K.E., Pickart, R.S., Selz, V., Mills, M.M., Pacini, A., Lewis, K.M., Joy-Warren, H.L.,
845 Nobre, C., van Dijken, G.L., Grondin, P.L., Ferland, J., and Arrigo, K.R. 2018. Under-
846 Ice Phytoplankton Blooms Inhibited by Spring Convective Mixing in Refreezing Leads.
847 *J Geophys Res Oceans* **123**(1): 90–109. Blackwell Publishing Ltd.
848 doi:10.1002/2016JC012575.
- 849 Macias, D., Garcia-Gorriz, E., and Stips, A. 2018. Deep winter convection and phytoplankton
850 dynamics in the NW Mediterranean Sea under present climate and future (horizon 2030)
851 scenarios. *Sci Rep* **8**(1). Nature Publishing Group. doi:10.1038/s41598-018-24965-0.
- 852 Marshall, J., and Schott, F. 1999. Open-ocean convection: Observations, theory, and models.
853 *Reviews of Geophysics* **37**(1): 1–64. doi:10.1029/98RG02739.
- 854 Marshall, K.N., Levin, P.S., Essington, T.E., Koehn, L.E., Anderson, L.G., Bundy, A.,
855 Carothers, C., Coleman, F., Gerber, L.R., Grabowski, J.H., Houde, E., Jensen, O.P.,

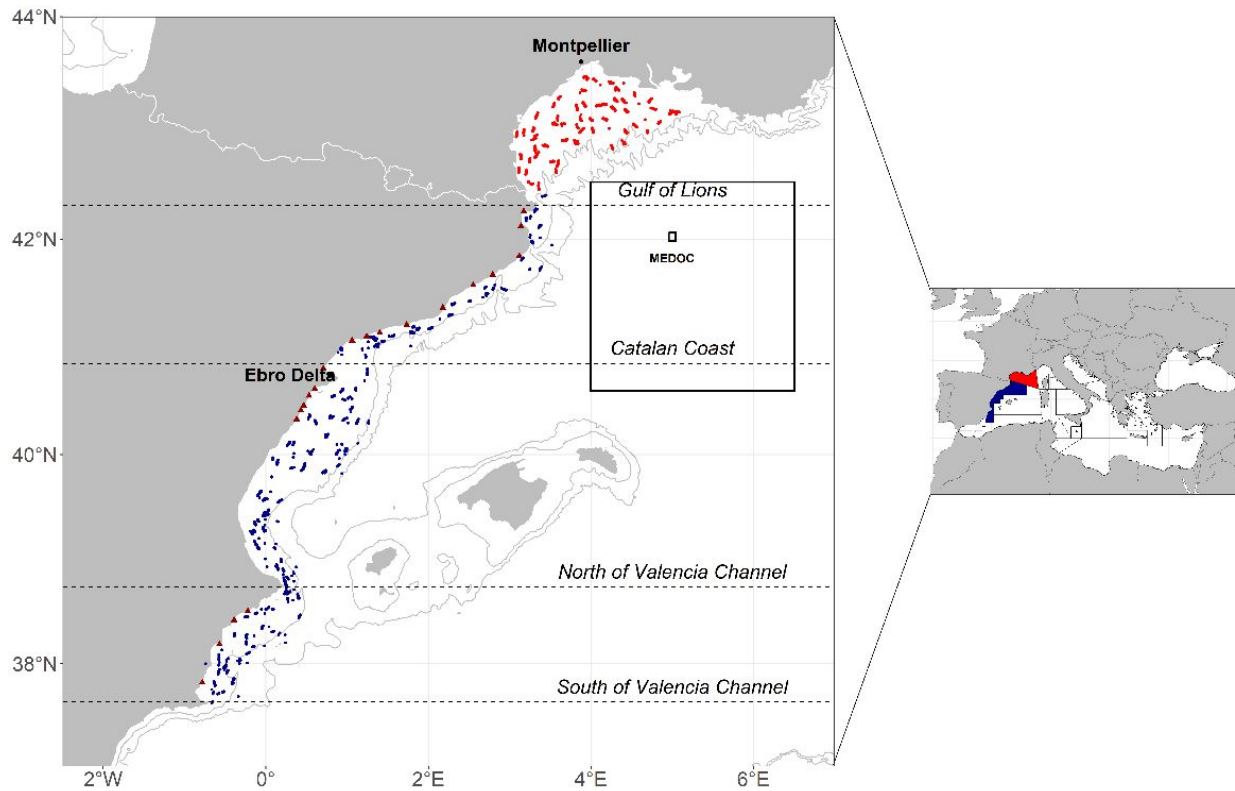
- 856 Möllmann, C., Rose, K., Sanchirico, J.N., and Smith, A.D.M. 2018. Ecosystem-Based
857 Fisheries Management for Social–Ecological Systems: Renewing the Focus in the
858 United States with Next Generation Fishery Ecosystem Plans. *Conserv Lett* **11**(1).
859 Wiley-Blackwell. doi:10.1111/conl.12367.
- 860 Martin, P., Maynou, F., Recasens, L., and Sabatés, A. 2016. Cyclic fluctuations of blue
861 whiting (*Micromesistius poutassou*) linked to open-sea convection processes in the
862 northwestern Mediterranean. *Fish Oceanogr* **25**(3): 229–240. Blackwell Publishing Ltd.
863 doi:10.1111/fog.12147.
- 864 Martín, P., Sabatés, A., Lloret, J., and Martin-Vide, J. 2012. Climate modulation of fish
865 populations: The role of the Western Mediterranean Oscillation (WeMO) in sardine
866 (*Sardina pilchardus*) and anchovy (*Engraulis encrasicolus*) production in the north-
867 western Mediterranean. *Clim Change* **110**(3–4): 925–939. doi:10.1007/s10584-011-
868 0091-z.
- 869 Martin-Vide, J., and Lopez-Bustins, J.A. 2006. The Western Mediterranean Oscillation and
870 rainfall in the Iberian Peninsula. *International Journal of Climatology* **26**(11): 1455–
871 1475. doi:10.1002/joc.1388.
- 872 Massutí, E., Monserrat, S., Oliver, P., Moranta, J., López-Jurado, J.L., Marcos, M., Hidalgo,
873 M., Guijarro, B., Carbonell, A., and Pereda, P. 2008. The influence of oceanographic
874 scenarios on the population dynamics of demersal resources in the western
875 Mediterranean: Hypothesis for hake and red shrimp off Balearic Islands. *Journal of*
876 *Marine Systems* **71**(3–4): 421–438. doi:10.1016/j.jmarsys.2007.01.009.
- 877 Matic-Skoko, S., Šegvić-Bubić, T., Mandić, I., Izquierdo-Gomez, D., Arneri, E., Carbonara,
878 P., Grati, F., Ikica, Z., Kolutari, J., Milone, N., Sartor, P., Scarcella, G., Tokaç, A., and
879 Tzanatos, E. 2018. Evidence of subtle genetic structure in the sympatric species *Mullus*
880 *barbatus* and *Mullus surmuletus* (Linnaeus, 1758) in the Mediterranean Sea. *Sci Rep*
881 **8**(1). Nature Publishing Group. doi:10.1038/s41598-017-18503-7.
- 882 MEDOC Group (1970) Observation of formation of deep water in the Mediterranean Sea,
883 1969. *Nature* **227**:1037–1040.
- 884 Mertens, C., and Schott, F. (1998). Interannual Variability of Deep-Water Formation in the
885 Northwestern Mediterranean. *Journal of physical oceanography*, **28**(7), pp.1410-1424.
- 886 Millot, C. 1990. The gulf of Lions' hydrodynamics. *Continental shelf research*, **10**(9-11), 885-
887 894.
- 888 Molinero, J.C., Ibanez, F., Nival, P., Buecher, E., and Souissi, S. 2005. Molinero, Juan
889 Carlos, Frédéric Ibanez, Paul Nival, Emmanuelle Buecher, and Sami Souissi. The North
890 Atlantic climate and the northwestern Mediterranean plankton variability. *Limnol.*
891 *Oceanogr.*, **50**(4), 2005, 1213–1220. *In* *Limnol. Oceanogr.* Available from
892 www.pml.ac.uk/.
- 893 Morfin, M., Bez, N., and Fromentin, J.M. 2016. Habitats of ten demersal species in the Gulf
894 of Lions and potential implications for spatial management. *Mar Ecol Prog Ser* **547**:
895 219–232. Inter-Research. doi:10.3354/meps11603.
- 896 Nye, J.A., Baker, M.R., Bell, R., Kenny, A., Kilbourne, K.H., Friedland, K.D., Martino, E.,
897 Stachura, M.M., Van Houtan, K.S., and Wood, R. 2014. Ecosystem effects of the
898 Atlantic Multidecadal Oscillation. *Journal of Marine Systems* **133**: 103–116. Elsevier.
899 doi:10.1016/j.jmarsys.2013.02.006.

- 900 Ordines, F., Lloret, J., Tugores, P., Manfredi, C., Guijarro, B., Jadaud, A., Porcu, C., de Sola,
 901 L.G., Carlucci, R., Sartini, M., Isajlović, I., and Massutí, E. 2019. A new approach to
 902 recruitment overfishing diagnosis based on fish condition from survey data. *Sci Mar*
 903 **83**(S1): 223–233. CSIC Consejo Superior de Investigaciones Científicas.
 904 doi:10.3989/scimar.04950.03A.
- 905 Ottersen, G., Planque, B., Belgrano, A., Post, E., Reid, P.C., and Stenseth, N.C. 2001.
 906 Ecological effects of the North Atlantic Oscillation. *Oecologia*, 128, pp.1-14.
 907 doi:10.1007/s004420100655.
- 908 Paradinas, I., Conesa, D., López-Quílez, A., Esteban, A., López, L.M.M., Bellido, J.M., and
 909 Pennino, M.G. 2020. Assessing the spatiotemporal persistence of fish distributions: A
 910 case study on two red mullet species (*mullus surmuletus* and *m. barbatus*) in the
 911 westernmediterranean. *Mar Ecol Prog Ser* **644**: 173–185. Inter-Research.
 912 doi:10.3354/meps13366.
- 913 Paradinas, I., Giménez, J., Conesa, D., López-Quílez, A., and Pennino, M.G. 2022. Evidence
 914 for spatiotemporal shift in demersal fishery management priority areas in the western
 915 Mediterranean. *Canadian Journal of Fisheries and Aquatic Sciences*. Canadian Science
 916 Publishing. doi:10.1139/cjfas-2021-0327.
- 917 Perry, A.L., Low, P.J., Ellis, J.R., and Reynolds, J.D. 2005. Climate Change and Distribution
 918 Shifts in Marine Fishes. Available from <https://www.science.org>.
- 919 Puerta, P., Quetglas, A., and Hidalgo, M. 2016. Seasonal variability of cephalopod
 920 populations: a spatio-temporal approach in the Western Mediterranean Sea. *Fish*
 921 *Oceanogr* **25**(4): 373–389. Blackwell Publishing Ltd. doi:10.1111/fog.12159.
- 922 Punt, A.E. 2019. Spatial stock assessment methods: A viewpoint on current issues and
 923 assumptions 1 2. *Fisheries Research*, 213, pp.132-143.
- 924 Punt, A.E. 2023. Those who fail to learn from history are condemned to repeat it: A
 925 perspective on current stock assessment good practices and the consequences of not
 926 following them. *Fish Res* **261**. Elsevier B.V. doi:10.1016/j.fishres.2023.106642.
- 927 Punt, A.E., Dunn, A., Elvarsson, B.P., Hampton, J., Hoyle, S., Maunder, M.N., Methot, R.D.,
 928 and Nielsen, A. 2020. Essential Features of the Next-Generation Integrated Fisheries
 929 Stock Assessment Package: A Perspective 2. *Fisheries Research*, 229, p.105617.
- 930 Reiss, H., Hoarau, G., Dickey-Collas, M., and Wolff, W.J. 2009. Genetic population structure
 931 of marine fish: Mismatch between biological and fisheries management units. *Fish and*
 932 *Fisheries* **10**(4): 361–395. doi:10.1111/j.1467-2979.2008.00324.x.
- 933 Rufener, M.C., Kristensen, K., Nielsen, J.R., and Bastardie, F. 2021. Bridging the gap
 934 between commercial fisheries and survey data to model the spatiotemporal dynamics of
 935 marine species. *Ecological Applications* **31**(8). Ecological Society of America.
 936 doi:10.1002/eap.2453.
- 937 Sabatés, A., Zaragoza, N., and Raya, V. 2015. Distribution and feeding dynamics of larval red
 938 mullet (*Mullus barbatus*) in the NW Mediterranean: The important role of cladocera. *J*
 939 *Plankton Res* **37**(4): 820–833. Oxford University Press. doi:10.1093/plankt/fbv040.
- 940 Sánchez Lizaso, J.L., Goñi, R., Reñones, O., García Charton, J.A., Galzin, R., Bayle, J.T.,
 941 Sánchez Jerez, P., Perez Ruzafa, A., and Ramos, A.A. 2000. Density dependence in
 942 marine protected populations: A review. doi:10.1017/S0376892900000187.

- 943 Schlenker, L.S., Stewart, C., Rock, J., Heck, N., and Morley, J.W. 2023. Environmental and
944 climate variability drive population size of annual penaeid shrimp in a large lagoonal
945 estuary. *PLoS One* **18**(5 May). Public Library of Science.
946 doi:10.1371/journal.pone.0285498.
- 947 Scientific, Technical and Economic Committee for Fisheries (STECF) – Stock Assessments:
948 demersal stocks in the western Mediterranean Sea (STECF-21-11). Publications Office
949 of the European Union, Luxembourg, 2021, EUR 28359 EN, ISBN 978-92-76-46116-6,
950 doi:10.2760/046729, JRC127744
- 951 Scientific, Technical and Economic Committee for Fisheries (STECF) – Evaluation of
952 maximum catch limits and closure areas in the Western Mediterranean (STECF-22-01).
953 EUR 28359 EN, Publications Office of the European Union, Luxembourg, 2021, ISBN
954 978-92-76-51980-5, doi:10.2760/657891, JRC129243.
- 955 Shelton, A.O., Thorson, J.T., Ward, E.J., and Feist, B.E. 2014. Spatial semiparametric models
956 improve estimates of species abundance and distribution. *Canadian Journal of Fisheries
957 and Aquatic Sciences* **71**(11): 1655–1666. Canadian Science Publishing.
958 doi:10.1139/cjfas-2013-0508.
- 959 Sparre, P., & Venema, S. C. 1998. Introduction to fish stock assessment. Part 1: Manual. FAO
960 Fisheries Technical Paper, 306(1).
- 961 Spedicato, M.T., Massutí, E., Mérigot, B., Tserpes, G., Jadaud, A., and Relini, G. 2019. The
962 medits trawl survey specifications in an ecosystem approach to fishery management. *Sci
963 Mar* **83**(S1): 9–20. CSIC Consejo Superior de Investigaciones Científicas.
964 doi:10.3989/scimar.04915.11X.
- 965 Spedicato, M.T., Cannas, R., Mahe, K., Morales, B., Tsigenopoulos, C., Zane, L., Kavadas,
966 S., Maina, I., Scarcella, G., Sartor, P. and Bandelj, V., 2021. Study on advancing
967 fisheries assessment and management advice in the Mediterranean by aligning
968 biological and management units of priority species. MED_UNITS.
- 969 Di Stefano, M., Legrand, T., Di Franco, A., Nerini, D., and Rossi, V. 2023. Insights into the
970 spatio-temporal variability of spawning in a territorial coastal fish by combining
971 observations, modelling and literature review. *Fish Oceanogr* **32**(1): 70–90. John Wiley
972 and Sons Inc. doi:10.1111/fog.12609.
- 973 Stenseth, N.C., and Mysterud, A. 2005, November. Weather packages: Finding the right scale
974 and composition of climate in ecology. doi:10.1111/j.1365-2656.2005.01005.x.
- 975 Szuwalski, C.S., and Hollowed, A.B. 2016. Climate change and non-stationary population
976 processes in fisheries management. *In* ICES Journal of Marine Science. Oxford
977 University Press. pp. 1297–1305. doi:10.1093/icesjms/fsv229.
- 978 Szuwalski, C.S., Vert-Pre, K.A., Punt, A.E., Branch, T.A., and Hilborn, R. 2015. Examining
979 common assumptions about recruitment: A meta-analysis of recruitment dynamics for
980 worldwide marine fisheries. *Fish and Fisheries* **16**(4): 633–648. Blackwell Publishing
981 Ltd. doi:10.1111/faf.12083.
- 982 Thorson, J.T. 2018. Three problems with the conventional delta-model for biomass sampling
983 data, and a computationally efficient alternative. *Canadian Journal of Fisheries and
984 Aquatic Sciences* **75**(9): 1369–1382. Canadian Science Publishing. doi:10.1139/cjfas-
985 2017-0266.

- 986 Thorson, J.T. 2019a. Guidance for decisions using the Vector Autoregressive Spatio-
 987 Temporal (VAST) package in stock, ecosystem, habitat and climate assessments. *Fish*
 988 *Res* **210**: 143–161. Elsevier B.V. doi:10.1016/j.fishres.2018.10.013.
- 989 Thorson, J.T. 2019b. Measuring the impact of oceanographic indices on species distribution
 990 shifts: The spatially varying effect of cold-pool extent in the eastern Bering Sea. *Limnol*
 991 *Oceanogr* **64**(6): 2632–2645. Wiley Blackwell. doi:10.1002/lno.11238.
- 992 Thorson, J.T., Arimitsu, M.L., Barnett, L.A.K., Cheng, W., Eisner, L.B., Haynie, A.C.,
 993 Hermann, A.J., Holsman, K., Kimmel, D.G., Lomas, M.W., Richar, J., and Siddon, E.C.
 994 2021. Forecasting community reassembly using climate-linked spatio-temporal
 995 ecosystem models. *Ecography* **44**(4): 612–625. Blackwell Publishing Ltd.
 996 doi:10.1111/ecog.05471.
- 997 Thorson, J.T., Ciannelli, L., and Litzow, M.A. 2020a. Defining indices of ecosystem
 998 variability using biological samples of fish communities: A generalization of empirical
 999 orthogonal functions. *Prog Oceanogr* **181**. Elsevier Ltd.
 1000 doi:10.1016/j.pocean.2019.102244.
- 1001 Thorson, J.T., Cheng, W., Hermann, A.J., Ianelli, J.N., Litzow, M.A., O’Leary, C.A., and
 1002 Thompson, G.G. 2020b. Empirical orthogonal function regression: Linking population
 1003 biology to spatial varying environmental conditions using climate projections. *Glob*
 1004 *Chang Biol* **26**(8): 4638–4649. Blackwell Publishing Ltd. doi:10.1111/gcb.15149.
- 1005 Thorson, J.T., Scheuerell, M.D., Shelton, A.O., See, K.E., Skaug, H.J., and Kristensen, K.
 1006 2015. Spatial factor analysis: A new tool for estimating joint species distributions and
 1007 correlations in species range. *Methods Ecol Evol* **6**(6): 627–637. British Ecological
 1008 Society. doi:10.1111/2041-210X.12359.
- 1009 Trochta, J.T., Pons, M., Rudd, M.B., Krigbaum, M., Tanz, A., and Hilborn, R. 2018.
 1010 Ecosystem-based fisheries management: Perception on definitions, implementations,
 1011 and aspirations. *PLoS One* **13**(1). Public Library of Science.
 1012 doi:10.1371/journal.pone.0190467.
- 1013 Tserpes, G., Massutí, E., Fiorentino, F., Facchini, M.T., Viva, C., Jadaud, A., Joksimovic, A.,
 1014 Pesci, P., Piccinetti, C., Sion, L., Thasitis, I., and Vrgoc, N. 2019. Distribution and
 1015 spatio-temporal biomass trends of red mullets across the mediterranean. *Sci Mar* **83**(S1):
 1016 43–55. CSIC Consejo Superior de Investigaciones Científicas.
 1017 doi:10.3989/scimar.04888.21A.
- 1018 Tsikliras, A.C., Licandro, P., Pardalou, A., McQuinn, I.H., Gröger, J.P., and Alheit, J. 2019.
 1019 Synchronization of Mediterranean pelagic fish populations with the North Atlantic
 1020 climate variability. *Deep Sea Res 2 Top Stud Oceanogr* **159**: 143–151. Elsevier Ltd.
 1021 doi:10.1016/j.dsr2.2018.07.005.
- 1022 Twiname, S., Audzijonyte, A., Blanchard, J.L., Champion, C., de la Chesnais, T., Fitzgibbon,
 1023 Q.P., Fogarty, H.E., Hobday, A.J., Kelly, R., Murphy, K.J., Oellermann, M., Peinado,
 1024 P., Tracey, S., Villanueva, C., Wolfe, B., and Pecl, G.T. 2020. A cross-scale framework
 1025 to support a mechanistic understanding and modelling of marine climate-driven species
 1026 redistribution, from individuals to communities. *Ecography* **43**(12): 1764–1778.
 1027 Blackwell Publishing Ltd. doi:10.1111/ecog.04996.
- 1028 Ulses, C., Estournel, C., De Madron, X. D., & Palanques, A. 2008. Suspended sediment
 1029 transport in the Gulf of Lions (NW Mediterranean): Impact of extreme storms and
 1030 floods. *Continental shelf research*, 28(15), 2048-2070. Vandenbulcke, L., and Barth, A.

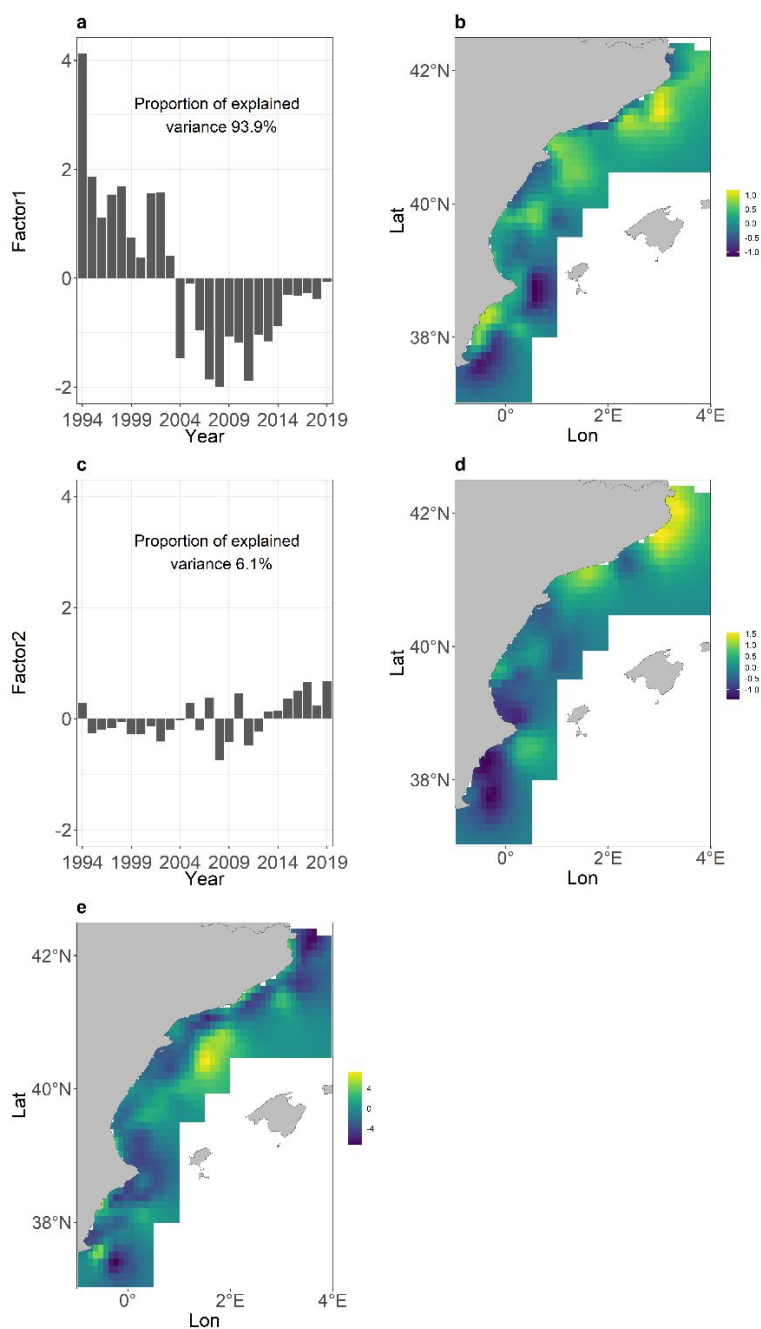
- 1031 2019. Upscaling of a local model into a larger-scale model. *Ocean Science* **15**(2): 291–
1032 305. Copernicus GmbH. doi:10.5194/os-15-291-2019.
- 1033 Vilas, D., Pennino, M.G., Bellido, J.M., Navarro, J., Palomera, I., and Coll, M. 2020.
1034 Seasonality of spatial patterns of abundance, biomass, and biodiversity in a demersal
1035 community of the NW Mediterranean Sea. *ICES Journal of Marine Science* **77**(2): 567–
1036 580. Oxford University Press. doi:10.1093/icesjms/fsz197.
- 1037 Zimmermann, F., Claireaux, M., and Enberg, K. 2019. Common trends in recruitment
1038 dynamics of north-east Atlantic fish stocks and their links to environment, ecology and
1039 management. *Fish and Fisheries* **20**(3): 518–536. Blackwell Publishing Ltd.
1040 doi:10.1111/faf.12360.
- 1041 Zuur, A.F., Tuck, I.D., and Bailey, N. 2003a. Dynamic factor analysis to estimate common
1042 trends in fisheries time series. *Canadian Journal of Fisheries and Aquatic Sciences*
1043 **60**(5): 542–552. doi:10.1139/F03-030.
- 1044 Zuur, A.F., Fryer, R.J., Jolliffe, I.T., Dekker, R., and Beukema, J.J. 2003b. Estimating
1045 common trends in multivariate time series using dynamic factor analysis.
1046 *Environmetrics* **14**(7): 665–685. doi:10.1002/env.611.
- 1047

1 **Figures**

2

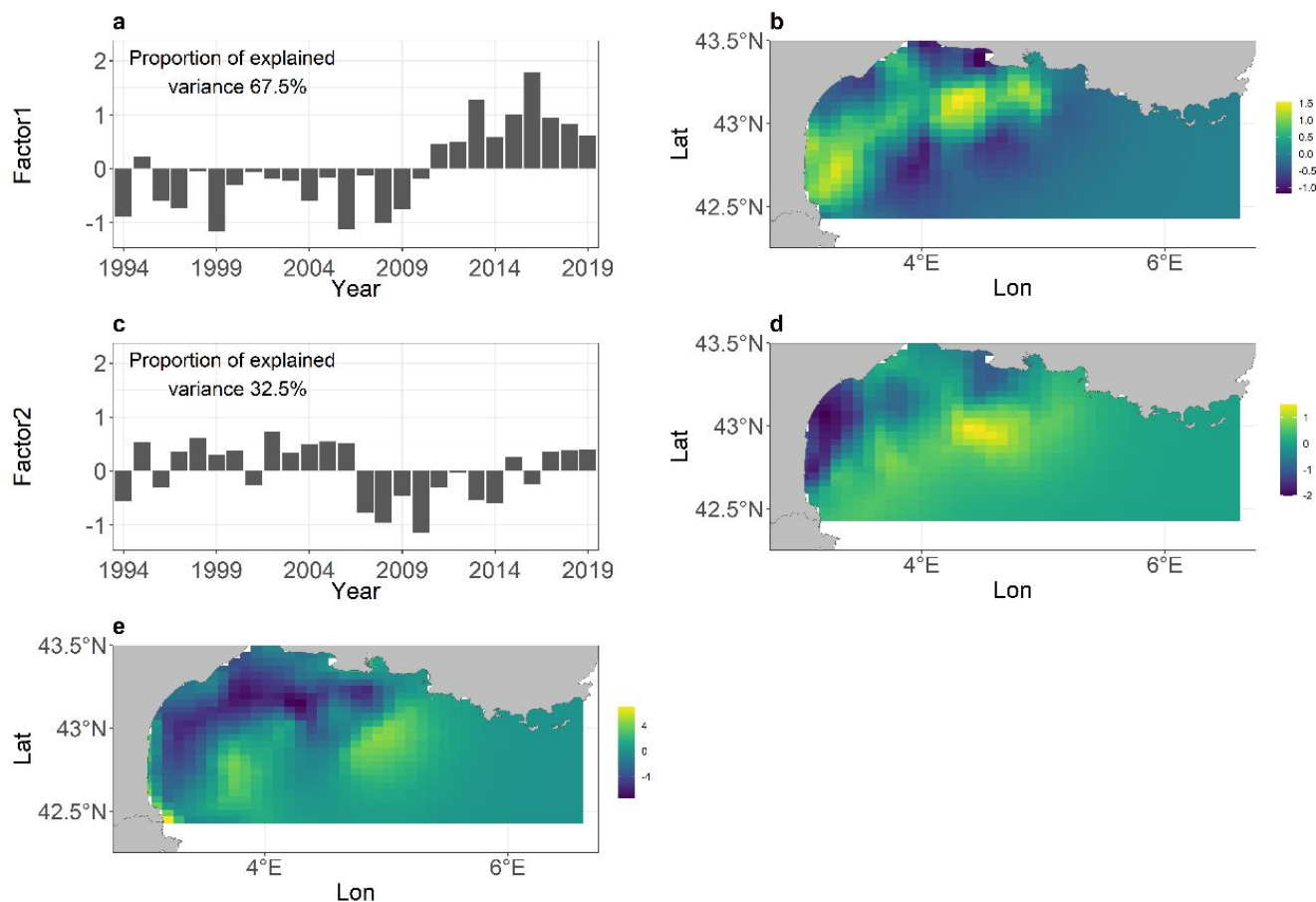
3 **Figure 1.** Study area encompassing the Geographic Subareas 6 (GSA06, in dark blue) and 7
 4 (GSA07, in red). Dark blue and red dots correspond to the MEDITS hauls in GSA06 and
 5 GSA07, respectively. The three subregions that GSA06 was subdivided into in this study are
 6 also shown: South of Valencia Channel, North of Valencia Channel and Catalan Coast. The 20
 7 ports (dark red triangles) that were used for the Dynamic Factor Analysis (DFA) and the 200
 8 and 1000 bathymetric contours (light grey lines) are also depicted. The two polygons around
 9 the MEDOC point that were used to calculate the Mixed Layer Depth (MLD) are present too.
 10 Map projection is WGS84 UTM.

11



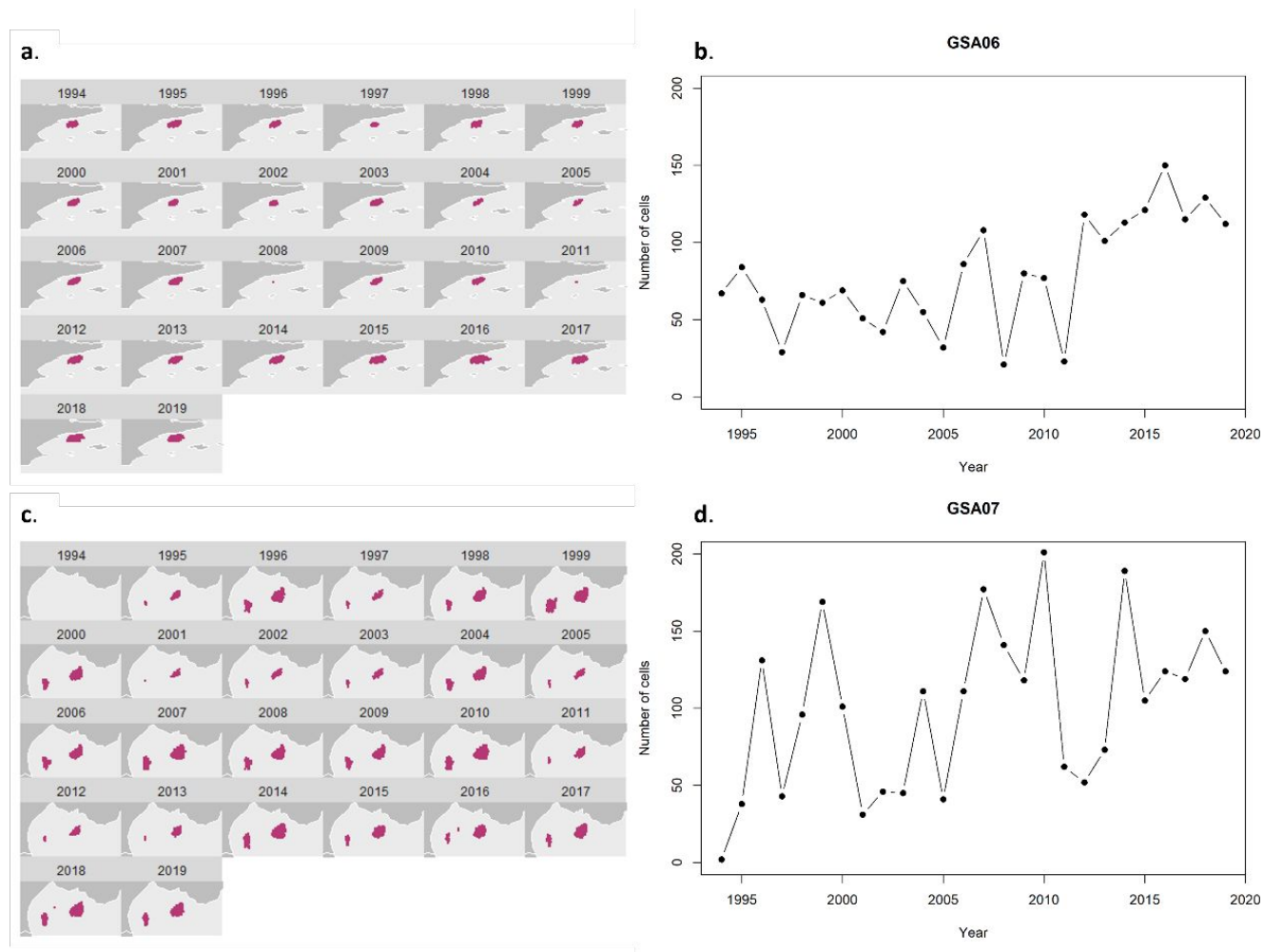
12

13 **Figure 2.** Portrayal of (a, c) the two dominant modes (factors) of density spatiotemporal
 14 variability for the Spanish Coast (GSA06), (b, d) the spatial maps associated with the two
 15 modes, and (e) the spatial variation ω which depicts the long-term average spatial pattern of
 16 red mullet density. For each axis (a, c), the proportion of explained variance is indicated. In
 17 panels b and d, yellow and blue tones represent areas which are associated with the positive
 18 and negative phase of the mode of variability, respectively. In the panel e, yellow and blue tones
 19 represent high- and low-density areas. Map projection is WGS84 UTM.



20

21 **Figure 3.** Portrayal of (a, c) the two dominant modes (factors) of density spatiotemporal
 22 variability for the Gulf of Lions (GSA07), (b, d) the spatial maps associated with the positive
 23 phase of the two modes, and (e) the spatial variation ω which depicts the long-term average
 24 spatial pattern of red mullet density. For each axis (a, c), the proportion of explained variance
 25 is indicated. In panels b and d, yellow and blue tones represent areas which are associated with
 26 the positive and negative phase of the mode of variability, respectively. In the panel e, yellow
 27 and blue tones represent high- and low-density areas. Map projection is WGS84 UTM.

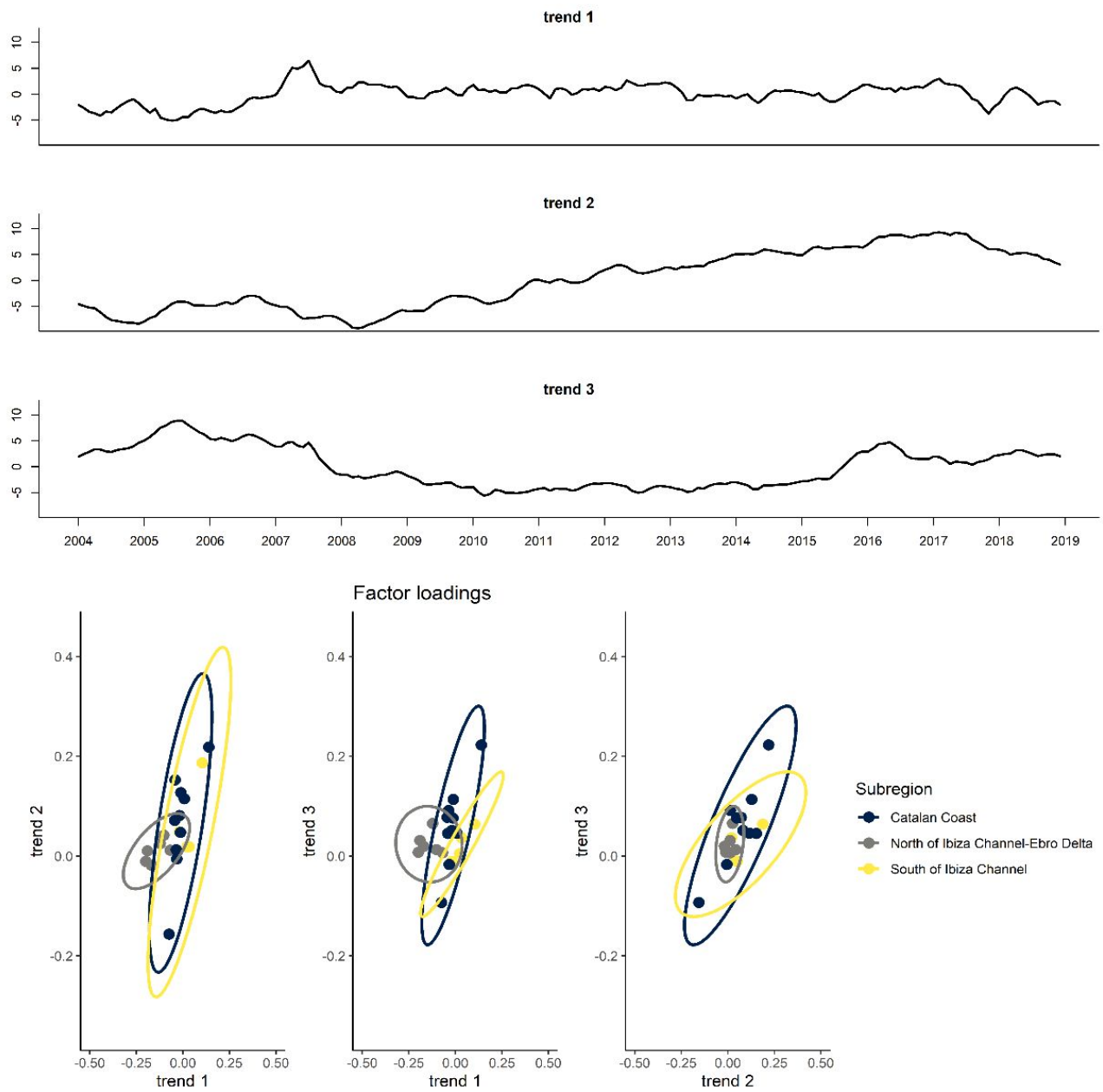


28

29 **Figure 4.** Spatial fluctuations of areas with densities higher than the 95% quantile and the
 30 respective time series in (a, b) the Spanish Coast and (c, d) the Gulf of Lions.

31

32



33

34 **Figure 5.** Results of the best model of Dynamic Factor Analysis (DFA) for landings per unit

35 effort (LPUE) time series in the Spanish Coast. (a) Common trends, (b) Factor loadings.

36

Table 1. Summary of the environmental variables that were used in this study. The period for which the information was available, the models that the variable was included, and the references are given in the table.

Env. variable	Years	Model	Reference
<i>Large-scale climatic indices</i>			
AMO	1994-2019	EOF & DFA	NOAA – Physical Sciences Laboratory
NAO	1994-2019	EOF & DFA	NOAA – National Centers for Environmental Prediction
WeMOi	1994-2019	EOF & DFA	Martin-Vide and Lopez-Bustins (2006)
<i>Regional & local indices</i>			
Chl-a	1998-2019	EOF & DFA	E.U. Copernicus Marine Service Information
SST	1994-2019	EOF & DFA	E.U. Copernicus Marine Service Information
LCI	1994-2019	EOF & DFA	Molinero <i>et al.</i> , 2005
Ebro runoff	1994-2019	EOF & DFA	Ebro Hydrographic Confederation
MLD	1994-2019	EOF	E.U. Copernicus Marine Service Information

AMO: Atlantic Multidecadal Oscillation; NAO: North Atlantic Oscillation; WeMOi: Western Mediterranean Oscillation index; Chl-a: Chlorophyll-a; SST: Sea Surface Temperature; LCI: Local Climatic Index; MLD: Mixed layer Depth; EOF: generalization of Empirical Orthogonal Function (with a spatiotemporal model); DFA: Dynamic Factor Analysis; NOAA: National Oceanic and Atmospheric Administration

Table 2. Summary of the best models with a significant environmental effect for each mode of spatiotemporal variability, and Geographic Sub-Area (GSA), and lag-k years, where k:0,1,2. In the case where the difference in AIC between the best two models was below 2 ($\Delta AIC < 2$), the second-best model is also reported in the table. The direction of the effect is also provided. The number of years of the data that was used in each model as well as the total number of fitted models depending on the number of environmental covariates for each GSA are shown in the right column.

Mode of spatiotemporal variability	Environmental variables of the best model	Lag	AIC	Number of years (Total number of fits)
GSA06				
1	AMO (+)	1	57.41	25 (16)
1	Ebro runoff (-)	2	56.56	24 (16)
1	MLD (Dec-Feb) (+)	2	57.99	24 (16)
GSA07				
1	SST_GSA07 (Dec-Feb) (-)	0	48.61	26 (12)
1	AMO (-)	0	50.04	26 (12)
2	MLD (Dec-Feb) (+)	1	41.41	25 (12)
2	WeMOi (-)	2	40.08	24 (12)

GSA06: Geographic Sub-Area 06; GSA07: Geographic Sub-Area 07; AIC: Akaike Information Criterion; AMO: Atlantic Multidecadal Oscillation; MLD: Mixed layer Depth; SST: Sea Surface Temperature; WeMOi: Western Mediterranean Oscillation index; (+): positive effect; (-): negative effect.

Table 3. Summary of the models with different combinations of the covariance matrix structure of observation errors (R) and the number of trends (m). The models are presented in ascending order, based on the correction to Akaike Information Criterion (AICc).

R	m	AICc
unconstrained	3	8760
unconstrained	2	8841
unconstrained	1	8934
diagonal and unequal	3	9044
diagonal and unequal	2	9179
equalvarcov	3	9184
diagonal and equal	3	9229
equalvarcov	2	9296
diagonal and equal	2	9349
diagonal and unequal	1	9415
equalvarcov	1	9461
diagonal and equal	1	9513